Lithos 240–243 (2016) 16–33

Contents lists available at ScienceDirect

Lithos

journal homepage: www.elsevier.com/locate/lithos

The Late Cretaceous I- and A-type granite association of southeast China: Implications for the origin and evolution of post-collisional extensional magmatism

Jiao-Long Zhao [a,1], Jian-Sheng Qiu [a,*], Liang Liu [a,b,1], Rui-Qiang Wang [a,1]

[a] State Key Laboratory for Mineral Deposits Research, School of Earth Sciences and Engineering, Nanjing University, Nanjing 210023, China
[b] State Key Laboratory of Ore Deposit Geochemistry, Institute of Geochemistry, Chinese Academy of Sciences, Guiyang 550081, China

ARTICLE INFO

Article history:
Received 15 July 2015
Accepted 15 October 2015
Available online 10 November 2015

Keywords:
I- and A-type granites
Petrogenesis
Magma mixing
Post-collisional extension
Coastal northeastern Zhejiang Province, SE China

ABSTRACT

We present new geochronological, mineralogical, and geochemical data for granitic plutons that crop out within the Zhoushan archipelago, northeastern coastal Zhejiang Province, in order to constrain their origin, and the genetic relationship between the I- and A-type granites. These granites can be divided into two groups: (1) the northern I-type Putuoshan (PTS) and Dadong'ao (DDA) plutons; and (2) the southern A-type Daqingshan (DQS), Taohuadao (THD), and Xiazhidao (XZD) plutons. Zircon LA–ICP–MS U–Pb dating yielded ages of 98–96 Ma for the northern I-type plutons and 89–86 Ma for the southern A-type plutons. All of these granites are highly siliceous, K-rich, and have similar total alkali and total rare earth element (REE) abundances. However, there are also geochemical differences between the I-type and the A-type granites. The northern I-type alkali-feldspar granites are high-K calc-alkaline, metaluminous to mildly peraluminous, contain low concentrations of the high field strength elements (HFSE; e.g., Nb, Ta, Zr, and Hf), and have low Ga/Al ratios (2.04–2.44). In contrast, the southern A-type granites are peralkaline and F-rich, and have lower CaO and Al_2O_3 concentrations, and higher $Fe_2O_3^T$ and HFSE concentrations and Ga/Al ratios (3.25–3.86). Meanwhile, they have slightly higher heavy REE (HREE) concentrations, and are more depleted in Ba, Sr, P, Ti, and Eu than the northern I-type granites. Both the I- and A-type granites have homogeneous whole-rock Nd and highly variable zircon Hf isotopic compositions. Of note, the southern peralkaline A-type granites appear to have more radiogenic Nd and Hf isotope compositions than the northern I-type granites. The present data, together with the results of a previous study on mafic enclaves within the PTS pluton, suggest that the northern I-type alkali-feldspar granites were generated by mixing of mantle-derived material with crustal-derived magmas that formed by dehydration melting of mica-bearing basaltic rocks, leaving a granulite residue in the lower crust. Both the I- and A-type granites were emplaced during post-collisional extensional tectonism associated with rollback of the steeply subducting paleo-Pacific Plate. An increase of the dip angle of the subducted palaeo-Pacific plate between the Early and Late Cretaceous resulted in enhanced extension, further thinning the lithosphere and causing more intensive underplating of mantle-derived magmas. This generated high temperatures and caused the partial melting of the residual granulite material, producing relatively anhydrous F-bearing felsic melts. The mixing of these unusual crustal melts with more voluminous mantle-derived mafic magmas generated the parental magmas that eventually formed the peralkaline A-type granites.

1. Introduction

Granitic rocks are intensively studied because they form in a variety of tectonic settings and thus provide important clues to the growth and reworking of continental crust and to regional tectonics and geodynamic processes (Goodege and Vervoort, 2006; Heilimo et al., 2014; Kemp and Hawkesworth, 2003). Although mantle-derived melts are involved in the genesis of some granitic magma, crustal recycling is still thought to be the dominant factor that controls the geochemical compositions of granitic rocks. Chappell and White (1974) proposed an I- and S-type granite classification scheme that relates granites to source rock compositions and suggested that I-type granites are mainly metaluminous and are generally derived from meta-igneous source rocks, whereas S-type granites are strongly peraluminous and generated by the partial melting of metasedimentary source material. The term "A-type granite" was subsequently defined by Loiselle and Wones (1979) to include a spectrum of alkali-rich granitic rocks that are characterized by high $Na_2O + K_2O$ concentrations, high Ga/Al ratios, and enrichments in Nb, Ta, Zr, and Hf (Collins et al., 1982; Whalen et al., 1987). A-type granites are derived from various source rocks by a variety of processes, and are genetically linked to extensional tectonism (Bonin, 2007;

* Corresponding author. Tel.: +86 25 89686824; fax: +86 25 83686016.
E-mail addresses: jlz2007@yeah.net (J.-L. Zhao), jsqiu@nju.edu.cn (J.-S. Qiu), liuliang0830@126.com (L. Liu), vickwrq2008@163.com (R.-Q. Wang).
[1] Tel.: +86 25 89686824; fax: +86 25 83686016.

http://dx.doi.org/10.1016/j.lithos.2015.10.018
0024-4937/

Karsli et al., 2012; Martin et al., 1994; Zhao et al., 2008). I-, S-, and A-type granites are not formed randomly but instead are closely connected to the tectonic setting and geodynamic evolution of an area (Barbarin, 1999; Eby, 1992; Whalen et al., 1987). Some of these types of granite are closely associated in space and time, forming complexes containing multiple granite suites (Breiter, 2012; Farahat et al., 2007; He et al., 2010; Jiang et al., 2011; Landenberger and Collins, 1996; Zhao et al., 2008), thus enabling reconstruction of the crustal evolution of an area and the tectonic setting. Such lithological associations are also important in unraveling the origin of A-type granites, which remains debated (Dall'Agnol et al., 2005; Frost and Frost, 2011; King et al., 1997; Qiu et al., 2004).

The late Mesozoic geology of SE China is characterized by widespread granitic intrusive and extrusive magmatism (Zhou and Li, 2000; Zhou et al., 2006). Granitoids in the coastal regions of SE China are predominantly I-type with lesser A-type, and both types commonly coexist as composite granitic complexes. Such complexes, including the Qingtian, Fuzhou, and Zhangzhou complexes, occur sporadically along the Changle–Nan'ao Fault (Fig. 1). Many studies have examined these coastal granites in recent decades and there is a general consensus that most originated from the mixing of crust- and mantle-derived magmas (Chen et al., 2013; Li et al., 2014b; Qiu et al., 2004; Xie et al., 2004; Xu et al., 1999a; Zhang et al., 2005). However, their magma sources, and the genetic relation between the I- and A-type granites remain debated (Chen et al., 2013; Dong and Peng, 1994; Martin et al., 1994; Qiu et al., 1999). In addition, although the late Mesozoic magmatism in SE China is thought to be related to subduction of the paleo-Pacific plate (Li et al., 2014b; Zhou et al., 2006; Zhu et al., 2010), details of the petrogenetic processes and geodynamic mechanisms involved in the generation of the I- and A-type granites in the coastal regions of Fujian and Zhejiang provinces remain poorly constrained.

This study focuses on a typical I- and A-type granite complex within the Zhoushan archipelago in coastal northeastern Zhejiang Province (Fig. 1). The complex consists of the northern I-type Putuoshan (PTS), and Dadong'ao (DDA) alkali-feldspar granites, and the southern A-type Daqingshan (DQS), Taohuadao (THD), and Xiazhidao (XZD) peralkaline granites (Fig. 2). Previous research by Xie et al. (2004) and Zhang et al. (2005) provided detailed whole-rock geochemical and mineralogical data for enclaves within the PTS pluton, indicating that these enclaves are calc-alkaline, have dioritic to monzonitic compositions, and probably formed by the crystallization of a more mafic remnant magma that was injected into an intermediate–acid magma chamber. Here, we present new mineralogical, geochronological, geochemical, and radiogenic isotope data for the granitic rocks of these five plutons, and use these data to: (1) determine the nature of the sources for the I- and A-type granites, (2) determine the genetic relationship between these granites, and (3) develop a tectonomagmatic model for the origin and evolution of both I- and A-type granites in SE China.

2. Geological background

The South China Block is located on the eastern margin of Eurasia and is bordered by the Qinling–Dabie orogenic belt to the north, the Tibetan Block to the west, and the Indochina Block to the south. It is divided into two major Precambrian continental blocks, namely the Yangtze Block to the northwest and the Cathaysia Block to the southeast,

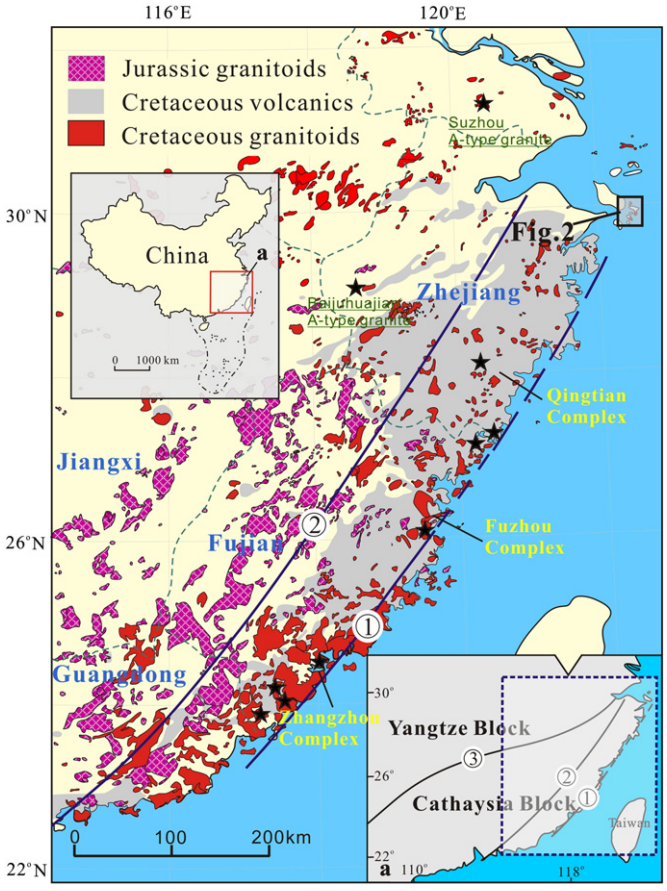

Fig. 1. Schematic map showing the distribution of the Yanshanian granitoids and volcanic rocks in SE China, in which study area is also shown (modified after Zhou et al., 2006). The localities of representative A-type granites in the coastal area are marked by black stars. Names of the fault zones: ① Changle–Nan'ao fault; ② Zhenghe–Dapu fault; ③ Jiangshan–Shaoxing fault.

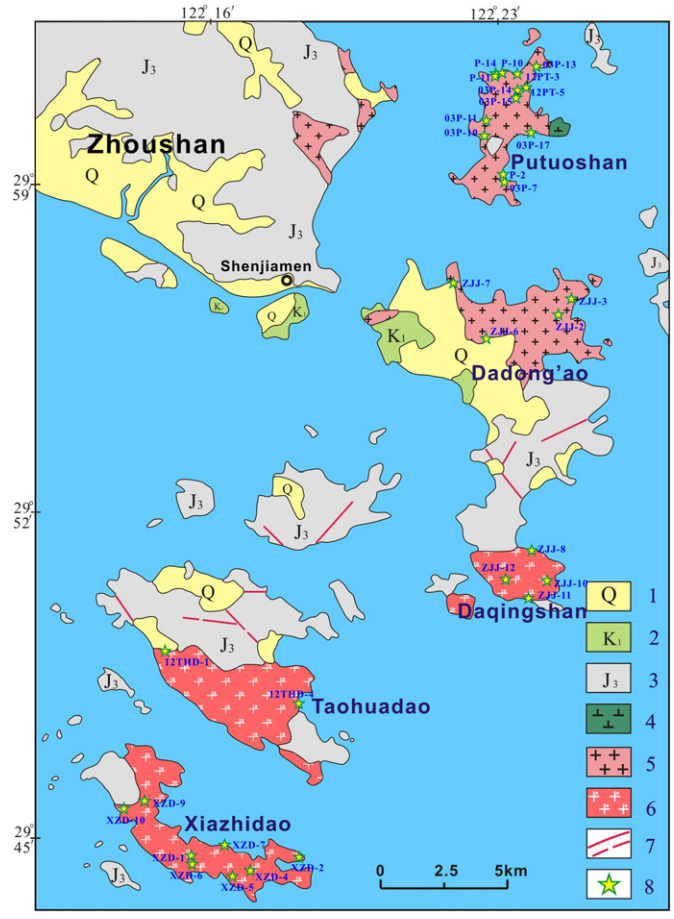

Fig. 2. Simplified geological map of the Zhoushan archipelago, coastal Zhejiang Province (modified after the 1:200,000 geological map of Dinghai and Shenjiamen Sheets). 1– Quaternary System; 2– Early Cretaceous Guantou Formation; 3– Late Jurassic Xishantou Formation; 4– quartz diorite porphyry; 5– alkali-feldspar granite; 6– peralkaline granite; 7– fault; 8– sample location.

separated by the Jiangshan–Shaoxing suture zone (Fig. 1a; Chen and Jahn, 1998; Zhang and Wang, 2007). The basement of the Cathaysia Block is dominated by Proterozoic rocks that are widely exposed in the southwestern parts of the block, including the ~1.8 Ga Badu complex in southwestern Zhejiang Province, and the ~0.8–0.7 Ga Mamianshan and Mayuan Groups in western Fujian Province (Li et al., 2014a; Yu et al., 2010). Systematic geological and geochemical research has indicated that the interior (western Cathaysia) and coastal (eastern Cathaysia) parts of the Cathaysia Block have different histories of crustal evolution and could be further separated into separate microcontinents, divided by the Zhenghe–Dabu Fault (Fig. 1; Chen and Jahn, 1998; Xu et al., 2007).

Late Mesozoic volcanic–intrusive magmatism was largely confined to the Cathaysia Block, with magmatic activity increasing from the interior to the coast (Zhou et al., 2006). The intrusive rocks are varied, comprising mainly high-K calc-alkaline I-type granite and lesser amounts of A-type granite, syenite, quartz diorite, and gabbro (He and Xu, 2012; Li et al., 2014b; Qiu et al., 2004; Zhou et al., 2006). The volcanic rocks in this area are generally rhyolitic and were predominantly erupted during the Cretaceous along the coastal area of SE China. Associated Cretaceous granitoids are also concentrated in the coastal region of SE China, generally along the Changle–Nan'ao Fault, whereas Jurassic intrusions are generally located inland (Fig. 1).

3. Petrography

The studied granites crop out in the Zhoushan archipelago of northeastern Zhejiang Province, geologically within the eastern margin of the Cathaysia Block. They occur in a roughly NNE–SSW-trending belt that contains five main plutons (from north to south): the Putuoshan, Dadong'ao, Daqingshan, Taohuadao, and Xiazhidao plutons (Fig. 2).

The PTS pluton crops out over an area of 26 km^2 on Putuo Island, and the eastern part of this pluton intruded a porphyritic Late Jurassic quartz diorite. The PTS pluton is dominated by an alkali-feldspar granite phase and a subordinate biotite alkali-feldspar granite phase. The intrusion is medium-grained and is faint red to gray in color (Fig. 3a). The major phases within the intrusion include quartz (30–35 vol.%), perthite (50–55 vol.%), plagioclase (10–15 vol.%), minor biotite and amphibole (<3 vol.%), and accessory zircon, apatite, and opaque oxide minerals. Plagioclase occurs as euhedral laths with well-developed polysynthetic

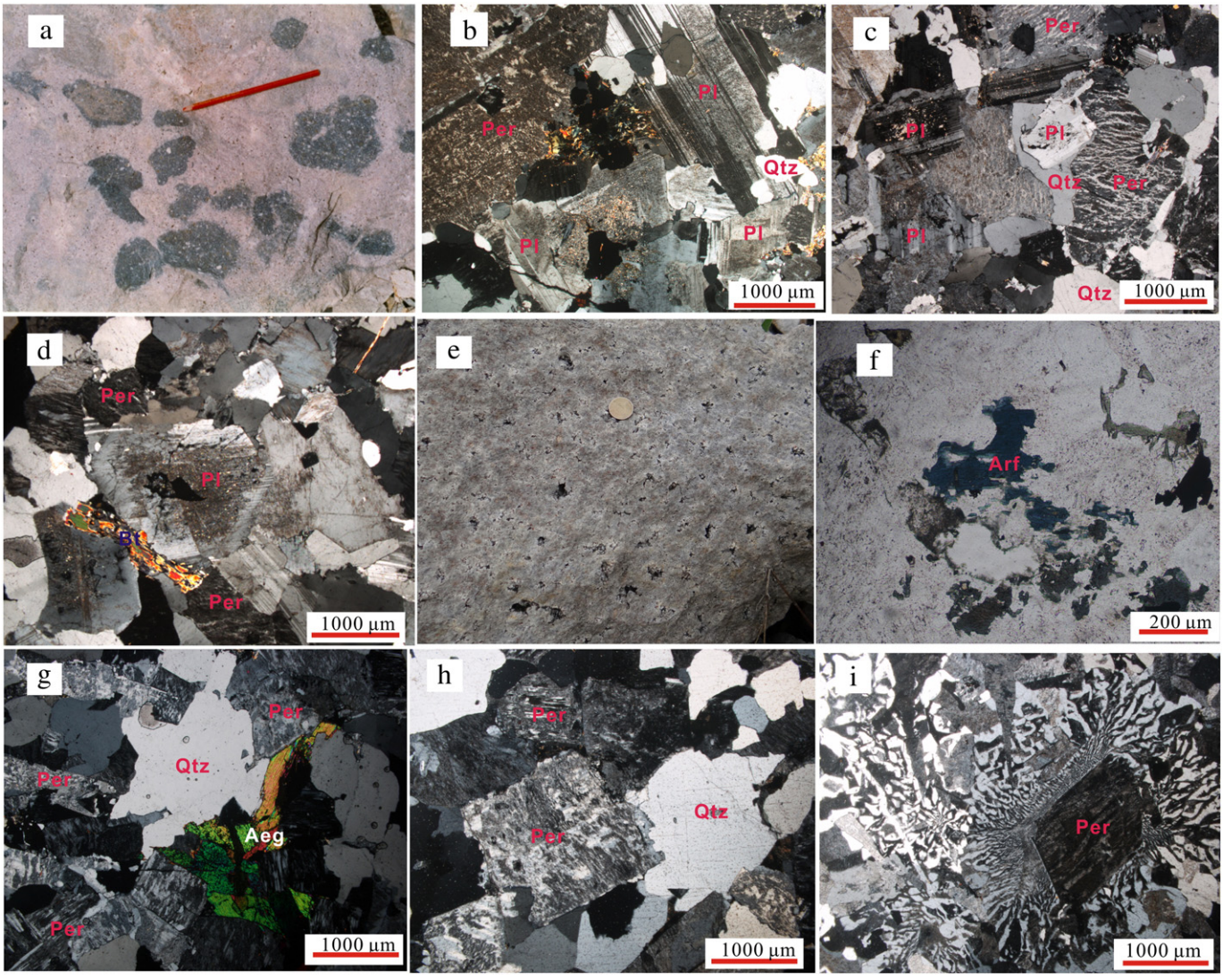

Fig. 3. (a) and (b) Macroscopic and thin section photos of alkali-feldspar granite from the Putuoshan pluton; (c) and (d) thin section photographs of representative alkali-feldspar granite from the Dadong'ao pluton; (e) miarolitic cavities in the Daqingshan pluton; (f) and (g) interstitial arfvedsonite and aegirine in the peralkaline granite from Daqingshan pluton; (h) thin section photograph of representative peralkaline granite from the Taohuadao pluton; (i) granophyric texture of peralkaline granite from the Xiazhidao pluton. Mineral abbreviation: Qtz– quartz; Per– perthite; Pl– plagioclase; Bt– biotite; Arf– arfvedsonite; Aeg– aegirine. (f), under plane-polarized light; other thin section photographs, under cross-polarized light.

Table 1
Summary of mineral assemblages, zircon U–Pb ages, Th/U ratios and Hf isotopic data for the studied granite samples in SE China Coast.

Sample	Pluton	GPS position	Main minerals	Age (Ma)	Th/U ratio	$\varepsilon_{Hf}(t)$
12PT-3	PTS	N30°01′24.0″ E122°23′32.6″	Qtz + Per + Pl + Bt + Amp	97.6 ± 0.9	1.10 ~ 4.12	-9.8 to -3.1
ZJJ-3	DDA	N29°56′34.0″ E122°24′58.9″	Qtz + Per + Pl + Bt + Amp	95.8 ± 1.0	0.89 ~ 4.04	-12.3 to -4.8
ZJJ-8	DQS	N29°51′08.9″ E122°23′46.3″	Qtz + Per + Pl + Bt + Aeg + Arf	88.1 ± 0.9	1.80 ~ 16.50	-7.7 to -3.1
12THD-1	THD	N29°49′05.0″ E122°14′45.6″	Qtz + Per + Pl + Bt + Aeg + Arf	88.6 ± 0.5	1.92 ~ 15.36	-7.4 to -1.7
12THD-4	THD	N29°47′52.7″ E122°18′10.1″	Qtz + Per + Pl + Bt + Aeg + Arf	89.2 ± 1.0	1.70 ~ 2.36	-7.5 to -2.2
XZD-2	XZD	N29°44′35.8″ E122°18′08.9″	Qtz + Per + Pl + Bt + Aeg + Arf	86.1 ± 0.8	2.09 ~ 8.04	-6.3 to -1.6

Mineral abbreviation: Qtz — quartz; Per — perthite; Pl — plagioclase; Bt — biotite; Arf — arfvedsonite; Aeg — aegirine.

twinning but is free of oscillatory zoning (Fig. 3b). The subhedral–anhedral biotite within the intrusion is generally interstitial to plagioclase and quartz. Microgranular mafic enclaves (MMEs) with spheroidal to ellipsoid–ovoid shapes are scattered throughout the granite, especially within the northern margin of the pluton (Fig. 3a).

The DDA pluton crops out over ~20 km^2 in northern Zhujiajian Island (Fig. 2) and consists mainly of an alkali-feldspar granite phase and a subordinate biotite alkali-feldspar granite phase, similar to the PTS pluton. The DDA granite is faint red to gray in color and has a medium-grained granitic texture. The pluton contains quartz (35–40 vol.%), perthite (50–55 vol.%), plagioclase (5–10 vol.%), and minor amounts of biotite (<5 vol.%). Plagioclase occurs as euhedral laths with well-developed polysynthetic twinning and is occasionally enclosed by quartz and perthite (Fig. 3c). Some plagioclase is clearly zoned with cores that are mottled and altered to sericite or kaolin. Biotite generally occurs interstitially, and some occurs as subhedral ragged flakes (Fig. 3d). MMEs are rare within the DDA intrusion.

The elliptical DQS pluton crops out over an area of ~7 km^2 within southern Zhujiajian Island. The granites within this pluton are leucocratic, ash-gray to pink in color, and have a medium-grained granitic texture. They contain perthite (60–65 vol.%), quartz (25–35 vol.%), alkali mafic minerals (e.g., arfvedsonite and aegirine, 3–5 vol.%), and minor amounts of magnetite, zircon, fluorite, apatite, and titanite, similar to the typical mineral association of peralkaline granites. Plagioclase is rarely observed. Alkaline amphiboles occur irregularly, interstitial to alkali feldspar and quartz (Fig. 3f), indicating late-stage crystallization. The alkaline pyroxenes within the granite commonly show pistachio-jasper pleochroism, and are generally not zoned (Fig. 3g). Miarolitic cavities (Fig. 3e) and granophyric texture are reasonably common but enclaves are rare.

The THD pluton crops out over an area of ~19 km^2 in southern Taohua Island (Fig. 2). The THD granite consists mainly of quartz (25–30 vol.%), and perthite (65–70 vol.%, Fig. 3h), along with minor amounts of arfvedsonite, aegirine, fluorite, magnetite, and zircon. Arfvedsonite within the intrusion is pleochroic and usually occurs interstitial to quartz and perthite, indicating an igneous origin. The THD pluton is similar to the DQS pluton in that miarolitic cavities and micrographic intergrowths of quartz and alkali feldspar are common, all of which are indicative of high-level emplacement (Mushkin et al., 2003). MMEs are rare within this pluton.

The XZD pluton crops out over an area of ~10 km^2 on Xiazhi Island (Fig. 2) and consists of a medium-grained granite that is dominated by perthite (65–70 vol.%) and quartz (25–30 vol.%), along with minor mafic minerals (<5 vol.%) such as biotite, arfvedsonite, and aegirine, and accessory magnetite, zircon, and fluorite. The perthite is subhedral to anhedral and contains fine, linear exsolution lamellae. Miarolitic cavities and granophyric texture (Fig. 3i) are reasonably common but enclaves are rare.

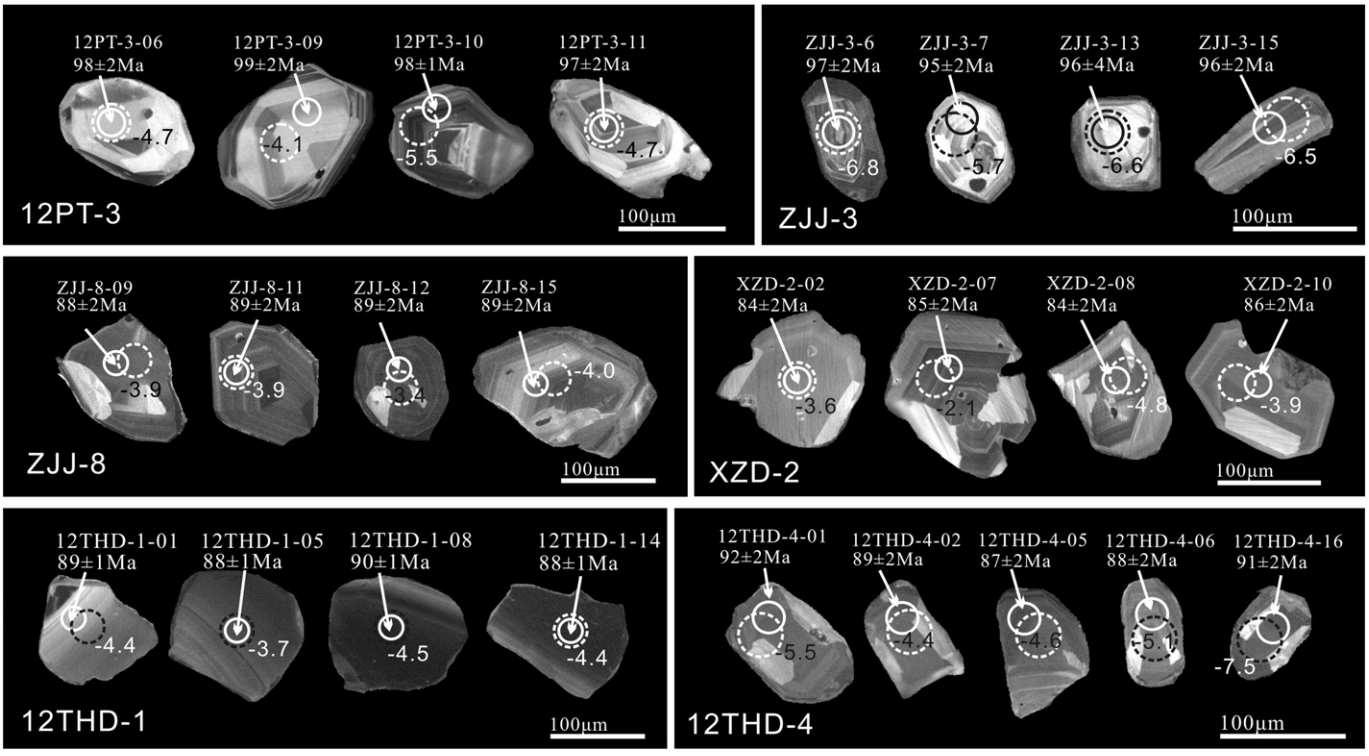

Fig. 4. CL images of the representative zircons from granites in the Zhoushan area, SE China. The morphology of zircon grains, $^{206}Pb/^{238}U$ ages, and $\varepsilon_{Hf}(t)$ values are shown. Small circles with solid line indicate the U–Pb dating positions, and large circles with dashed line indicate the sites of Hf isotope analyses.

In summary, the granitic plutons in the Zhoushan area can be divided into two groups according to field relations and petrography (Table 1): a northern group of alkali-feldspar granite plutons (including the PTS and DDA plutons) and a southern group of peralkaline granite plutons (including the DQS, THD, and XZD plutons).

4. Sampling and analytical methods

4.1. Zircon U-Pb dating and Hf isotopes

Zircons from six samples (12PT-3 for PTS, ZZJ-3 for DDA, ZJJ-8 for DQS, 12THD-1 and 12THD-4 for THD, and XZD-2 for XZD plutons) were separated by conventional techniques, including crushing, sieving, and magnetic and heavy liquid separation methods. Zircon grains, handpicked under a binocular stereomicroscope, were mounted in epoxy resin, and polished to expose their centers. Cathodoluminescence (CL) and optical microscopy images were taken to ensure that the least fractured and most inclusion-free zones of the zircons were analyzed. The CL images were obtained using a Mono CL3 + (Gatan, Pleasanton, CA, USA) attached to a scanning electron microscope (Quanta 400 FEG, Hillsboro, OR, USA) at the State Key Laboratory of Continental Dynamics, Northwest University, Xi'an, China.

Zircon U–Pb isotopic analyses were carried out using an Agilent 7500a ICP–MS coupled to a New Wave Research 213-nm laser ablation system at the State Key Laboratory for Mineral Deposits Research, Nanjing University. The ablated material was transported in a He carrier gas through PVC tubing (inner diameter, 3mm) and combined with argon in a 30-cm^3 mixing chamber prior to entry into the ICP–MS. Analyses were carried out using a beam diameter of 25 μm, a repetition rate of 5 Hz, and an energy of 23.74–26.68 J/cm^2. Date acquisition for each analysis took 100s (40 s on background signal, 60 s on ablated signal). A homogeneous standard zircon (GEMOC GJ-1: $^{207}Pb/^{206}Pb$ age of 608.5 ± 0.4 Ma and a relatively

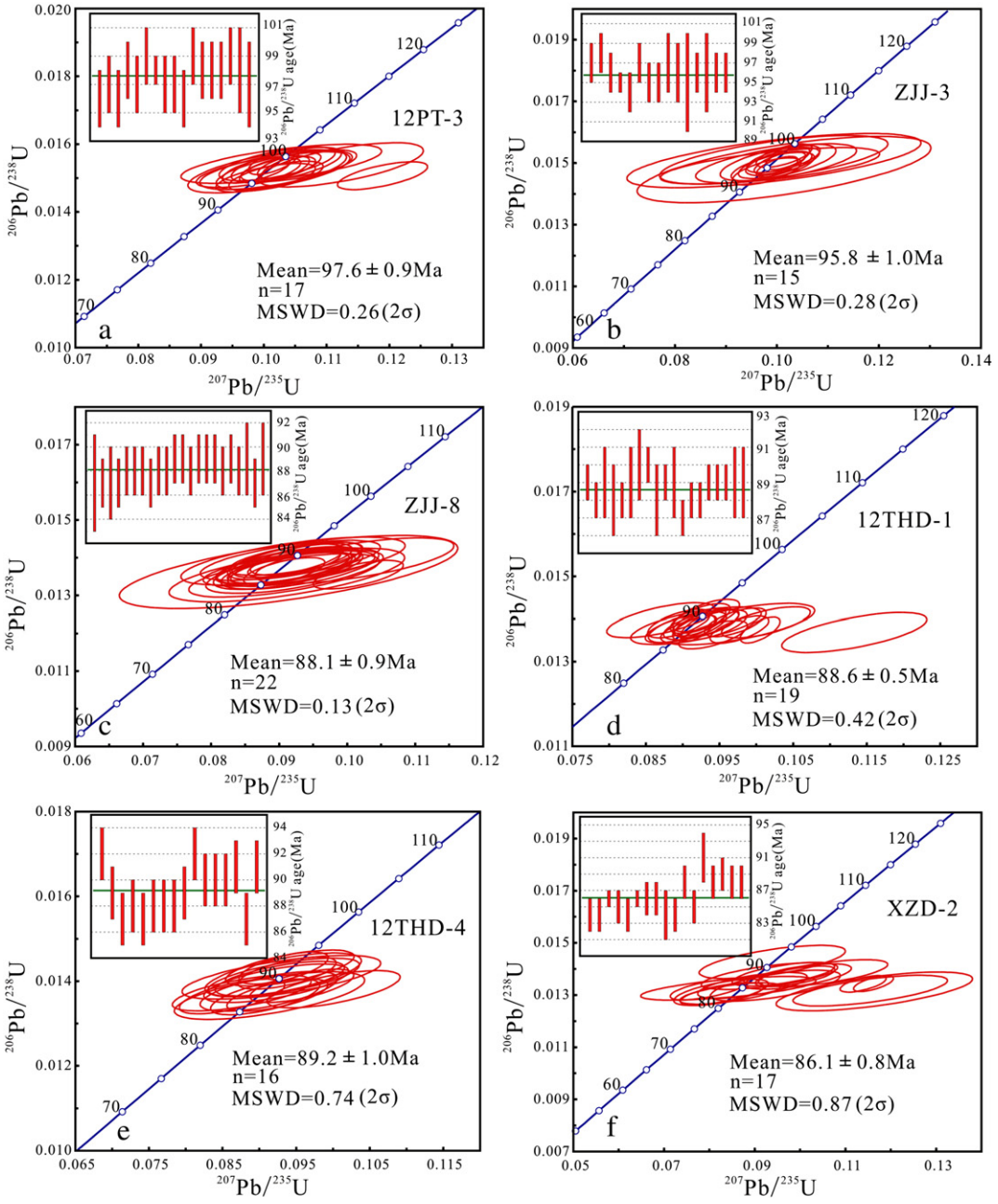

Fig. 5. Zircon U-Pb concordia diagrams and weighted mean $^{206}Pb/^{238}U$ ages for granitic rocks of the Putuoshan pluton (a), Dadong'ao pluton (b), Daqingshan pluton (c), Taohuadao pluton (d, e) and Xiazhidao pluton (f).

young $^{206}Pb/^{238}U$ age of 599.8 ± 4.5 Ma, Jackson et al., 2004) was used to correct the mass discrimination of the mass spectrometer and residual elemental fractionation. A well-characterized zircon standard (Mud Tank; intercept age, 732 ± 5 Ma; Black and Gulson, 1978) was used as an independent control on reproducibility and instrument stability. The raw ICP-MS U–Pb isotopic data were exported in ASCII format and processed using GLITTER 4.4 software (van Achterbergh et al., 2001). Common Pb corrections were performed using the method described by Andersen (2002). Mean age calculations and Concordia diagram plots were performed using Isoplot (version 2.49) (Ludwig, 2001).

In situ zircon Hf isotope analyses were performed using a Thermo Scientific Neptune Plus multi-collector (MC) ICP–MS attached to a New Wave UP193 solid-state laser ablation system at the State Key Laboratory for Mineral Deposits Research, Nanjing University. Zircons were ablated with a beam diameter of 35 μm, energy of 9.54–11.35 J/cm^2, an 8 Hz laser repetition rate, and with a 26 s laser ablation time. Two reference standards were also measured to evaluate the reliability of the data (Mud Tank zircon $^{176}Hf/^{177}Hf$ ratio = 0.282501 ± 0.000004, $n = 23, 2\sigma$ and 91500 zircon $^{176}Hf/^{177}Hf$ ratio = 0.282316 ± 0.000009, $n = 9, 2\sigma$) before analyses of unknown samples. The measured $^{176}Hf/^{177}Hf$ ratios of the two standards agree with the recommended values within 2σ error (Griffin et al., 2007).

4.2. Mineral chemistry

Quantitative analyses of the minerals were carried out using a JEOL JXA-8100 electron-microprobe (EMP) at the State key Laboratory for Mineral Deposits Research, Nanjing University, China, and were operated at an accelerating voltage of 15 kV, a beam current of 10 nA, and a beam diameter of 1μm.

4.3. Whole-rock major and trace element, and Nd isotope analyses

All samples selected for chemical and isotopic analyses were fresh, and were crushed and powdered to 200 mesh using an agate mill. Whole-rock major elements, trace elements, and Nd isotopic compositions were determined at the State key Laboratory for Mineral Deposits Research, Nanjing University, China. For major element analyses, mixtures of whole-rock powders (0.5 g) and $Li_2B_4O_7 + LiBO_2 + LiBr$ (11 g) were made into glass disks and then analyzed using a Thermo Scientific ARL 9900 X-ray fluorescence (XRF) spectrometer. The analytical precision was estimated to be less than 10% for all major elements and less than 1% for the majority of elements. For trace element analyses, ~50 mg of powder was dissolved in high-pressure Teflon bombs using a HF + HNO_3 mixture; Rh was used as an internal standard to monitor for signal drift during the ICP–MS analyses. Trace element concentrations were determined using a Finnigan Element II ICP–MS. Detailed analytical procedures followed Gao et al. (2003). The analytical precision was better than 10% for all trace elements, with the majority being better than 5%. Major and trace element compositions of the rock standard GSR-1 (Xie et al., 1989) and trace element compositions of the duplicate sample are shown in Appendix A.

For whole-rock Nd isotope analyses, ~50 mg of powder was dissolved in Teflon beakers with a HF + HNO_3 mixture, and Nd was then separated and purified using a cation-exchange resin with HIBA as the eluent. The detailed chemical separation and isotopic measurement procedures used are described in Pu et al. (2004, 2005). The isotopic compositions of the purified Nd solutions were determined on a Thermo Scientific Neptune Plus MC–ICP–MS. For the present analyses, the Nd isotopic ratios were corrected for mass fractionation by normalizing to $^{146}Nd/^{144}Nd = 0.7219$. During the analysis period, measurements of the Japan JNdi-1 Nd standard yielded a $^{143}Nd/^{144}Nd$ ratio of 0.512075 ± 0.000012 ($n = 11, 2\sigma$).

5. Analytical results

5.1. Zircon U–Pb ages and Hf isotopic compositions

Zircons from the granitic plutons are generally transparent, colorless to light yellow, euhedral, and prismatic. They range from 50 to 200 μm in size and have length/width ratios of 1:1–2:1. CL images of zircon grains used for LA-ICP-MS analysis show well-developed oscillatory zoning (Fig. 4). These zircon grains also show high and variable Th/U ratios (0.89–16.50), indicating a magmatic origin. The results of the

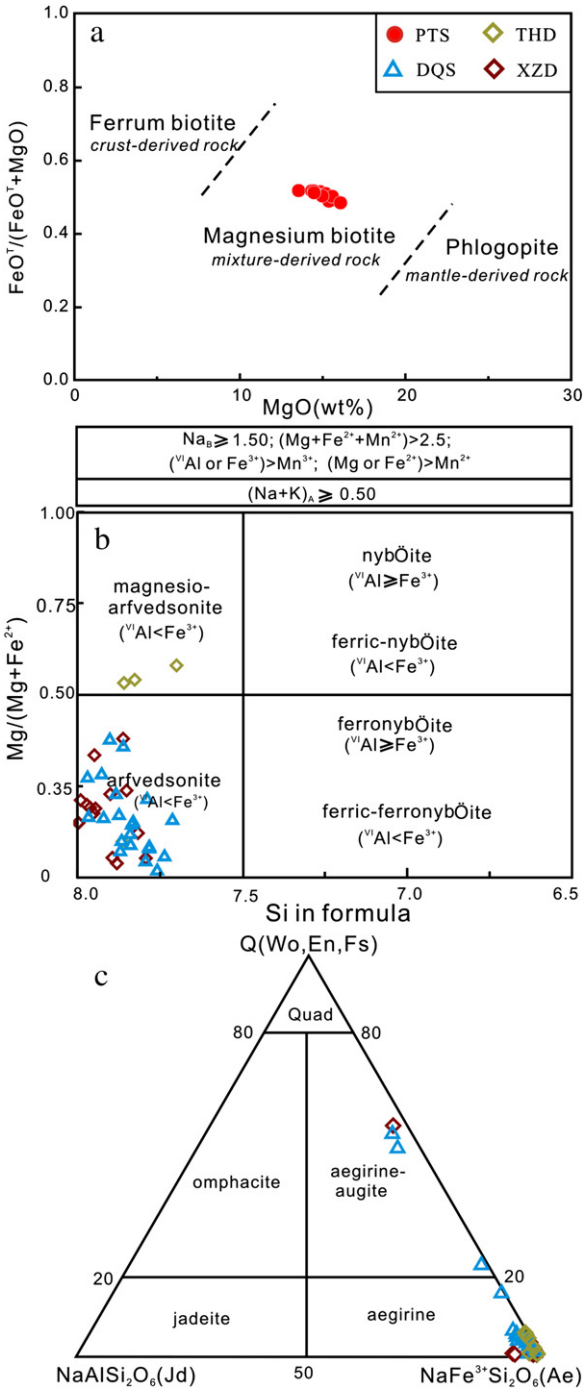

Fig. 6. (a) $FeO^T/(FeO^T + MgO)$ vs. MgO diagram for biotite (after Zhou, 1988); (b) Amphibole compositions from the Daqingshan, Taohuadao and Xiazhidao peralkaline granites (after Leake et al., 1997); (c) classification diagram of pyroxene (after Morimoto et al., 1988).

Table 2
Major (wt.%) and trace element (ppm) compositions of granites in the Zhoushan area, SE China.

Pluton	Putuoshan								Dadong'ao				Daqingshan			
Sample	12PT-3	12PT-5	03P-10	03P-11	03P-13	03P-14-3	03P-15	03P-17	ZJJ-2	ZJJ-3	ZJJ-6	ZJJ-7	ZJJ-8	ZJJ-10	ZJJ-11	ZJJ-12
Rock type	Alkali-feldspar granite												Peralkaline granite			
SiO_2	75.88	77.50	76.87	77.53	76.61	77.13	75.75	76.93	76.97	77.27	78.03	78.07	76.88	77.93	76.74	78.66
TiO_2	0.16	0.18	0.12	0.10	0.13	0.12	0.13	0.11	0.11	0.11	0.09	0.09	0.13	0.10	0.09	0.10
Al_2O_3	13.28	12.59	12.47	12.42	12.48	12.59	12.71	12.82	12.39	12.59	12.23	12.32	11.61	11.39	11.56	11.47
$Fe_2O_3^T$	1.05	1.14	0.70	0.66	0.86	0.86	0.91	0.83	0.70	0.73	0.45	0.60	1.37	0.95	1.33	1.09
MnO	0.10	0.10	0.05	0.05	0.05	0.03	0.06	0.08	0.07	0.07	0.05	0.07	0.14	0.01	0.02	0.08
MgO	0.40	0.36	0.01	0.01	0.05	0.03	0.06	0.07	0.23	0.26	0.19	0.22	0.23	0.22	0.20	0.20
CaO	0.87	0.51	0.45	0.40	0.64	0.41	0.81	0.56	0.51	0.49	0.36	0.44	0.20	0.23	0.20	0.06
Na_2O	4.22	4.35	4.02	3.88	4.08	4.20	4.06	4.13	4.17	4.16	4.05	4.17	4.64	4.07	4.06	4.35
K_2O	4.37	4.08	4.80	4.69	4.50	4.67	4.81	4.72	4.49	4.57	4.48	4.51	4.26	4.23	4.67	4.12
P_2O_5	0.03	0.02	0.01	0.01	0.01	0.01	0.01	0.01	0.01	0.01	0.01	0.01	0.01	0.01	0.01	0.01
LOI	0.83	0.69	0.37	0.64	0.20	0.37	0.70	0.44	0.57	0.50	0.59	0.43	0.50	0.96	0.63	0.62
Total	101.19	101.52	99.87	100.39	99.61	100.42	100.01	100.70	100.22	100.76	100.53	100.93	99.97	100.10	99.51	100.76
Sc	3.11	4.00	2.30	2.16	2.55	2.44	2.57	2.36	3.48	3.78	2.96	3.36	3.22	2.56	1.63	2.72
V	7.22	6.90	3.17	3.30	5.71	4.26	5.40	4.56	2.25	2.38	1.43	1.40	2.54	1.95	2.42	1.87
Ni	1.26	0.35	2.14	2.08	12.88	2.83	4.07	5.93	0.27	3.55	0.50	0.54	0.15	2.28	2.51	0.26
Ga	15.6	15.4	14.8	15.3	14.8	13.6	15.5	15.3	15.5	15.8	15.7	15.9	22.2	21.7	23.6	22.4
Cs	1.04	1.07	1.47	1.17	1.07	0.90	1.57	1.46	6.14	4.00	2.79	3.41	0.87	0.94	1.03	0.54
Rb	158	147	164	168	154	145	205	160	221	228	251	246	207	209	286	205
Ba	484	220	189	148	257	202	232	214	88.1	111	50.2	50.1	15.8	11.0	16.0	12.9
Th	19.7	25.1	22.1	25.8	21.4	23.2	23.2	24.5	25.8	26.6	26.4	27.2	16.5	16.4	28.7	23.8
U	5.06	3.35	3.18	3.54	2.70	3.51	6.28	4.32	3.73	5.29	5.51	3.94	4.99	4.27	19.44	5.96
Ta	1.36	1.98	1.43	1.77	1.17	1.30	1.76	1.98	1.18	1.49	1.43	1.38	2.15	1.93	3.03	2.61
Nb	15.5	20.4	16.5	21.1	13.9	15.0	21.0	22.6	24.9	27.8	27.1	27.7	47.2	46.8	47.3	38.3
Pb	22.2	19.0	24.5	29.7	18.2	21.1	33.8	24.2	20.9	21.5	22.8	21.8	9.88	14.5	20.9	46.0
Sr	113	58.1	30.0	45.0	58.0	108	49.0	54.0	34.0	36.8	28.4	21.4	4.76	8.25	18.9	4.09
Nd	23.8	31.0	18.4	15.8	18.7	17.0	20.0	14.8	15.8	16.5	13.3	12.1	13.5	9.17	19.3	7.06
Zr	134	140	95.0	77.5	90.9	91.2	83.3	85.2	79.9	91.4	79.9	76.1	299	180	306	310
Hf	4.79	5.68	3.41	3.25	3.08	3.59	3.30	3.22	3.66	4.15	3.69	3.82	12.4	7.70	13.1	12.8
Y	20.3	22.6	14.8	17.7	14.5	11.8	16.8	16.1	22.8	28.2	22.5	22.9	40.8	25.2	38.0	24.9
La	39.0	46.6	29.5	24.3	32.9	27.7	33.2	23.7	46.3	45.9	35.6	32.7	47.6	39.9	53.2	34.5
Ce	70.3	83.6	54.2	44.3	62.7	52.0	64.2	45.3	50.9	54.1	44.2	45.1	49.6	48.0	78.5	44.0
Pr	7.30	9.10	5.66	4.76	5.90	5.32	6.19	4.47	5.38	5.50	4.45	4.10	4.77	3.52	6.89	2.76
Nd	23.8	31.0	18.4	15.8	18.7	16.9	20.0	14.8	15.8	16.5	13.3	12.1	13.5	9.17	19.3	7.06
Sm	3.59	4.78	3.00	3.11	2.98	2.95	3.38	2.66	2.27	2.54	2.04	1.88	2.26	1.31	3.57	1.01
Eu	0.59	0.42	0.33	0.27	0.38	0.31	0.36	0.29	0.21	0.24	0.15	0.15	0.12	0.07	0.19	0.05
Gd	3.46	4.57	2.27	2.37	2.19	2.10	2.56	2.20	2.40	2.70	2.09	1.99	2.73	1.60	4.23	1.32
Tb	0.47	0.66	0.38	0.45	0.37	0.34	0.47	0.41	0.34	0.39	0.32	0.30	0.49	0.24	0.73	0.23
Dy	2.54	3.77	2.26	2.81	2.25	1.92	2.78	2.50	1.97	2.36	1.93	1.98	3.49	1.65	4.89	1.78
Ho	0.51	0.75	0.49	0.61	0.49	0.41	0.59	0.56	0.42	0.50	0.42	0.44	0.85	0.41	1.10	0.47
Er	1.67	2.38	1.42	1.75	1.40	1.16	1.72	1.59	1.44	1.72	1.45	1.54	3.13	1.56	3.96	1.97
Tm	0.26	0.38	0.25	0.32	0.24	0.21	0.29	0.30	0.24	0.29	0.25	0.27	0.58	0.30	0.74	0.42
Yb	1.82	2.63	1.71	2.14	1.71	1.47	2.03	1.89	1.76	2.08	1.89	2.03	4.41	2.37	5.77	3.57
Lu	0.30	0.41	0.28	0.34	0.28	0.24	0.32	0.30	0.29	0.34	0.31	0.34	0.75	0.42	0.98	0.64

Note: LOI: loss on ignition. Data for the MMEs in Putuoshan (PTS) pluton are from Zhang et al. (2005); * — Data from Qiu et al. (2004).

LA–ICP–MS U–Pb isotopic analyses (Supplementary table 1) are summarized in Table 1 and shown in Fig. 5. Zircon Hf isotopic analyses were performed on the same grains selected for zircon U–Pb dating. Lu–Hf isotopic compositions are given in Supplementary table 2.

5.1.1. Putuoshan pluton

Seventeen U–Pb analyses of zircons from the sample 12PT-3 define a weighted mean $^{206}Pb/^{238}U$ age of 97.6 ± 0.9 Ma (MSWD = 0.26, 2σ; Fig. 5a), which is considered the crystallization age of the PTS pluton. Nineteen Hf isotopic spot analyses undertaken on zircons from this sample yielded variable initial $^{176}Hf/^{177}Hf$ ratios (0.282527 to 0.282625) and $\varepsilon_{Hf}(t)$ values (−9.8 to −3.1) with a weighted mean value of −4.3 ± 0.6 (2σ). The corresponding two-stage T_{DM2} model ages are of 1.36–1.66 Ga.

5.1.2. Dadong'ao pluton

Fifteen analyses of zircons from the sample ZJJ-3 are concordant or nearly concordant, yielding $^{206}Pb/^{238}U$ ages of 94 ± 2 to 98 ± 2 Ma and a weighted mean $^{206}Pb/^{238}U$ age of 95.8 ± 1.0 Ma (MSWD = 0.28, 2σ; Fig. 5b). This age represents the crystallization age of the DDA alkali-feldspar granite and is within error of the age of the PTS pluton. Eighteen zircon Hf isotopic analyses yield initial $^{176}Hf/^{177}Hf$ ratios of 0.282576–0.282479 and $\varepsilon_{Hf}(t)$ values of –4.8 to –12.3, with corresponding two-stage T_{DM2} model ages of 1.47–1.67 Ga.

5.1.3. Daqingshan pluton

Twenty-two zircon grains from the peralkaline DQS granite (ZJJ-8) yield concordant $^{206}Pb/^{238}U$ ages that range from 87 ± 2 to 89 ± 2 Ma with a weighted mean age of 88.1 ± 0.9 Ma (MSWD = 0.13, 2σ; Fig. 5c). These zircons have more radiogenic Hf isotope compositions than the zircons from the PTS and DDA plutons, with initial $^{176}Hf/^{177}Hf$ ratios of 0.282629–0.282501, $\varepsilon_{Hf}(t)$ values of –3.1 to –7.7, and T_{DM2} model ages of 1.35–1.65 Ga.

5.1.4. Taohuadao pluton

Two samples from the THD pluton were analyzed during this study. Nineteen analyses of zircons from the sample 12THD-1 are all concordant or near-concordant and yield a weighted mean $^{206}Pb/^{238}U$ age of 88.6 ± 0.5 Ma (MSWD = 0.42, 2σ; Fig. 5d). Sixteen analyses from the sample 12THD-4 form a concordant group with a weighted mean $^{206}Pb/^{238}U$ age of 89.2 ± 1.0 Ma (MSWD = 0.74, 2σ; Fig. 5e). These two ages are the same within error, indicating a crystallization age of

Taohuadao						Xiazhidao								Average of MMEs in the PTS pluton
12THD-1	12THD-4	T-1*	T-3*	T-9*	T-10*	XZD-1	XZD-2	XZD-4	XZD-5	XZD-6	XZD-7	XZD-9	XZD-10	
Peralkaline granite														
78.45	78.20	77.80	76.48	77.00	77.00	77.47	77.37	76.56	77.22	77.54	77.71	76.82	77.41	60.00
0.10	0.12	0.09	0.12	0.11	0.09	0.11	0.16	0.14	0.14	0.15	0.13	0.13	0.13	0.90
11.55	11.83	11.38	11.49	11.58	11.53	11.59	11.66	11.70	11.75	11.88	11.81	11.90	11.79	16.35
1.11	0.92	1.67	1.68	1.66	1.79	0.86	1.04	1.19	1.02	1.01	0.96	1.08	0.88	6.46
0.08	0.04	0.11	0.12	0.14	0.13	0.01	0.02	0.10	0.10	0.05	0.03	0.06	0.03	0.24
0.22	0.19	0.08	0.07	0.08	0.01	0.19	0.23	0.23	0.23	0.21	0.20	0.22	0.18	2.17
0.20	0.08	0.49	0.52	0.49	0.35	0.07	0.18	0.08	0.16	0.21	0.17	0.07	0.28	4.63
4.27	4.26	4.06	4.26	3.80	4.74	4.26	4.22	4.25	4.27	4.46	4.44	4.20	4.41	4.40
4.28	4.53	4.32	4.37	4.73	4.43	4.44	4.57	4.56	4.59	4.58	4.52	4.61	4.40	2.52
0.01	0.01	0.01	0.01	0.01	0.01	0.00	0.00	0.02	0.01	0.00	0.00	0.01	0.00	0.42
0.69	0.58					0.64	0.84	0.68	0.71	0.75	0.59	0.77	0.62	
100.96	100.76					99.64	100.29	99.51	100.20	100.84	100.56	99.87	100.13	
2.50	2.17					2.95	3.29	3.43	3.42	3.35	3.29	2.45	2.89	15.4
2.59	1.79					1.11	2.17	1.78	1.65	1.64	1.32	1.81	1.78	140
0.29	1.10					4.72	1.60	1.01	0.77	0.50	1.24	0.67	3.46	4.94
21.1	20.4	20.8	22.6	21.2	21.2	21.3	22.0	22.3	22.8	21.5	20.6	20.7	20.4	20.5
1.06	1.20					0.93	0.52	1.51	0.86	0.86	0.79	1.40	0.66	3.13
223	172	208	241	196	187	196	199	195	190	199	147	188	190	92.8
10.9	12.7	72.0	48.0	42.0	34.0	15.1	1.66	1.51	2.50	0.75	0.05	7.05	1.15	750
16.0	13.3	12.2	18.9	14.9	16.0	15.1	17.8	20.2	18.3	26.3	13.3	16.8	17.4	9.26
2.31	1.78	4.60	1.10	3.50	3.40	2.36	3.56	4.30	2.38	4.42	2.10	2.88	3.42	1.15
1.96	1.47	2.58	2.01	2.31	2.22	1.47	1.75	2.24	1.50	1.76	1.24	1.80	1.76	1.17
46.2	40.1	37.0	32.0	32.0	33.0	34.8	30.0	35.3	26.3	30.5	21.5	44.4	30.1	13.0
28.4	12.5					44.0	25.4	33.1	18.7	16.6	21.0	13.3	36.1	20.6
9.70	4.83	4.90	15.0	5.20	8.00	7.38	2.21	2.98	6.91	3.15	0.48	4.35	2.59	692
11.1	14.0	15.5	13.8	22.8	23.7	19.0	23.2	14.5	30.1	21.6	14.8	14.9	16.5	40.4
186	137	245	244	251	276	188	279	348	210	255	138	231	244	208
8.04	5.36	7.20	7.60	6.20	7.40	7.12	9.44	12.58	7.53	9.29	5.44	9.33	9.39	
37.7	16.0	13.0	30.6	38.5	33.1	15.9	33.2	34.9	37.4	45.6	37.3	33.2	38.2	27.4
46.4	39.6	29.6	39.0	28.6	32.0	47.4	29.2	24.6	37.6	29.4	24.2	39.3	28.4	39.0
46.6	46.9	37.6	59.9	56.9	60.9	52.6	56.7	54.6	51.1	55.8	41.9	44.1	50.1	78.1
4.13	4.77	4.51	4.31	7.56	7.96	6.49	6.78	4.47	8.69	6.40	4.66	4.97	5.30	9.85
11.1	14.0	15.5	13.8	22.8	23.7	19.0	23.2	14.5	30.1	21.6	14.8	14.9	16.5	40.4
1.66	2.13	2.54	2.45	4.10	3.86	3.08	4.87	3.03	6.74	4.86	3.17	2.68	3.16	7.55
0.08	0.08	0.15	0.15	0.22	0.22	0.09	0.20	0.11	0.23	0.16	0.10	0.08	0.12	1.69
2.12	2.12	2.04	2.20	4.14	3.71	2.97	4.62	3.33	6.79	5.18	3.51	2.89	3.53	6.21
0.35	0.29	0.30	0.40	0.71	0.66	0.40	0.75	0.64	1.16	0.97	0.68	0.51	0.65	0.92
2.46	1.68	1.67	2.67	4.62	4.08	2.02	4.47	4.69	6.79	6.50	4.62	3.42	4.40	4.95
0.60	0.35	0.43	0.71	1.04	0.97	0.38	0.90	1.08	1.29	1.40	0.99	0.75	0.98	1.00
2.22	1.20	1.42	2.32	3.61	3.11	1.21	2.90	3.70	3.88	4.47	3.07	2.49	3.27	2.63
0.40	0.20	0.28	0.47	0.60	0.50	0.20	0.48	0.64	0.60	0.72	0.48	0.43	0.55	0.41
2.99	1.52	2.19	4.01	4.39	3.90	1.59	3.47	4.56	3.98	4.82	3.13	3.09	3.93	2.55
0.51	0.26	0.36	0.67	0.67	0.61	0.27	0.57	0.74	0.62	0.76	0.47	0.51	0.64	0.38

89 Ma for the THD peralkaline granite. Both samples have similar zircon Hf isotopic compositions with initial $^{176}Hf/^{177}Hf$ ratios of 0.282668–0.282532, $\varepsilon_{Hf}(t)$ values from –1.7 to –7.5, and corresponding T_{DM2} ages of 1.27–1.63 Ga.

5.1.5. Xiazhidao pluton

Seventeen analyses of zircons from the sample XZD-2 plot on or near the concordia, yielding a weighted mean $^{206}Pb/^{238}U$ age of 86.1 ± 0.8 Ma (MSWD = 0.87, 2σ; Fig. 5f) that we consider to indicate the crystallization age of the XZD pluton. Twenty zircon Hf isotopic analyses yield variable initial $^{176}Hf/^{177}Hf$ ratios of 0.282539–0.282674, $\varepsilon_{Hf}(t)$ values from –6.3 to –1.6, and T_{DM2} ages of 1.25–1.55 Ga.

5.2. Mineral chemistry

Representative microprobe analyses of major mineral phases within the granites in the Zhoushan area are listed in Supplementary tables 3–5 and shown in Fig. 6.

5.2.1. Biotite

Biotite within the PTS alkali-feldspar granite has rather homogeneous compositions with high MgO (13.55–16.53 wt.%) and moderate FeO^T (14.53–15.81 wt.%) concentrations. They have compositions close to the Mg-rich eastonite end-member, with relatively low Fe/(Fe + Mg) cationic ratios of 0.33–0.38, and thus belong to magnesium biotite (Fig. 6a).

5.2.2. Amphibole

The amphiboles within the PTS alkali-feldspar granite are calcic, have Ca_B values of >1.5, are enriched in Mg but depleted in Fe, and have Fe/(Fe + Mg) ratios of 0.24–0.34, indicating magnesio-hornblende compositions. The amphiboles within the DQS, THD, and XZD peralkaline granites are all sodic and can be further classified as arfvedsonite and minor magnesio-arfvedsonite using the classification of Leake et al. (1997) (Fig. 6b); the latter type is restricted to the THD pluton. These sodic amphiboles contain >3.17 wt.% F, with some amphiboles containing up to 5.09 wt.% F, distinctly higher than the concentrations within calcic amphiboles in the PTS alkali-feldspar granite (0.32–0.40 wt.% F).

5.2.3. Pyroxene

Pyroxene is only present within the DQS, THD, and XZD peralkaline granites. All of these pyroxenes are enriched in Na_2O (6.30–14.51 wt.%) and FeO^T (27.06–33.36 wt.%), and are depleted in MgO

(<5.57 wt.%) and CaO (<3.89 wt.%), indicating they are sodic pyroxenes. Further classification using the scheme of Morimoto et al. (1988) indicates that these pyroxenes are aegirines and aegirine–augites (Fig. 6c).

5.3. Whole-rock major and trace element geochemistry

The whole-rock major and trace element compositions of representative samples from the five plutons studied here are summarized in Table 2.

Both the alkali-feldspar granites and peralkaline granites have high and restricted SiO_2 contents (>74 wt.%) with D.I. (differentiation index) values of 93.4–98.1, indicating they are highly evolved. They both have similarly high K_2O contents in the range 4.08–4.81 wt.%, with K_2O/Na_2O values close to 1, and can be classified as high-K calc-alkaline rocks (Fig. 7a). In the plot of SiO_2 *vs.* A.R. (alkalinity ratio; Fig. 7b), all samples from the intrusions fall in the alkaline field, although the peralkaline granites tend to show much higher A.R. values than the alkali-feldspar granites. The peralkaline granites from the southern DQS, THD, and XZD plutons have relatively low concentrations of Al_2O_3 (11.38–11.90 wt.%), P_2O_5 (0.01–0.02 wt.%), and CaO (0.06–0.52 wt.%). Their total ($K_2O + Na_2O$) contents vary from 8.30 to 9.17 wt.%. On the A/CNK *vs.* A/NK diagram, they are mostly peralkaline with A/NK ratios of <1.0 (Fig. 7c), which is consistent with the presence of Na-rich mafic minerals (e.g., arfvedsonite and aegirine). In contrast, the alkali-feldspar granites from the northern PTS and DDA plutons have higher Al_2O_3 and CaO, and lower $Fe_2O_3^{tot}$ compared with the southern peralkaline granites. The majority of these rocks are metaluminous to weakly peraluminous with A/CNK values of 0.95–1.02, and only one sample is peraluminous (Fig. 7c). Following Sylvester (1989), the alkali-feldspar granites belong to highly fractionated granites, whereas the peralkaline granites straddle the boundary between the highly fractionated and alkaline fields (Fig. 7d).

All of the peralkaline and alkali-feldspar granite samples have similar total rare earth element ($\sum$REE) concentrations of 100.9–191.0 and 98.6–183.9 ppm, respectively. Their chondrite-normalized REE patterns are marked by significant LREE enrichments, nearly flat HREE patterns, and distinctly negative Eu anomalies (Fig. 8a and b). These granites have primitive-mantle-normalized multi-element variation patterns that are enriched in large ion lithophile element (LILE; e.g., Rb, Th, and U) and depleted in Ba, Sr, P, and Ti, suggesting these rocks formed from highly evolved magmas (Fig. 8c and d). Despite these similarities, there are also some differences in the compositions of the northern alkali-feldspar granites and southern peralkaline granites, with more significant depletions in Ba, Sr, P, Ti, and Eu, and greater enrichment in the HREE and the high field strength elements (HFSE; e.g., Nb, Ta, Zr, and Hf) in the latter (Fig. 8).

5.4. Whole-rock Sm–Nd isotopes

The whole-rock Nd isotopic compositions of the granites analyzed during this study are listed in Supplementary table 6 and are shown in Fig. 9a. All $\varepsilon_{Nd}(t)$ values and two-stage Nd model ages (T_{DM2}) were calculated using the crystallization ages obtained in this study, and they define two distinct groups: one corresponding to the alkali-feldspar granites within the PTS and DDA plutons, and the other associated with the peralkaline granites in the DQS, THD, and XZD plutons. The northern alkali-feldspar granites have homogeneous Nd isotopic compositions with initial $^{143}Nd/^{144}Nd$ ratios of 0.512129–0.512510, $\varepsilon_{Nd}(t)$ values from −7.5 to −7.1, and two-stage Nd model ages (T_{DM2}) of 1.47–1.51 Ga. In contrast, the southern peralkaline granites have slightly more radiogenic Nd isotopic compositions with initial $^{143}Nd/^{144}Nd$ ratios of 0.512191–0.512235, $\varepsilon_{Nd}(t)$ values from −5.7 to −6.5, and two-stage Nd model ages (T_{DM2}) of 1.35–1.42 Ga.

6. Discussion

6.1. Classification of alkali-feldspar granites and peralkaline granites within the Zhoushan archipelago

The geochemistry of A-, I-, and S-type granites is generally well known (Chappell, 1999; Chappell and White, 1974; Clemens, 2003; Ghani et al., 2013; Whalen et al., 1987). The fact that the granites in the present study area have relatively low A/CNK and K_2O/Na_2O values, low P_2O_5 concentrations, and are free of typical peraluminous minerals (e.g., cordierite, andalusite, and garnet) argue strongly that they are not S-type granites (Chappell, 1984; Chappell and White, 1974; Whalen et al., 1987; Zhao et al., 2015b). Their peralkaline chemical compositions and common occurrence of Na-rich mafic minerals (e.g., arfvedsonite and aegirine) indicate the southern peralkaline intrusions are typical A-type granites. In contrast, the northern alkali-feldspar granites are generally metaluminous to slightly peraluminous and have low HFSE concentrations. Biotites within the PTS alkali-feldspar granites have FeO^T/MgO ratios of 0.94–1.08, and can be classified as magnesian subvariety. All of the amphiboles from the PTS alkali-feldspar granites are calcic and have Ca_B values of >1.5. These characteristics indicate that the northern alkali-feldspar granites are typical I-type granites (Chappell, 1984; Whalen et al., 1987). These northern granites plot in the I-, S-, and M-type fields in Ga/Al *vs.* (Zr + Nb + Ce + Y) and Zr, Y, and Ce *vs.* Ga/Al discrimination diagrams (Fig. 10), whereas all of the southern peralkaline granites are solely classified as A-type granites. In summary, the PTS and DDA alkali-feldspar granites are classified as I-type, and the DQS, THD, and XZD peralkaline granites as A-type, and together they make up a typical composite I- and A-type granitic complex.

6.2. Petrogenesis of the I-type PTS and DDA alkali-feldspar granites

The alkali-feldspar granites from the PTS and DDA plutons are highly siliceous, calc-alkaline, and have typical I-type geochemical characteristics. They have relatively enriched bulk-rock Nd and zircon Hf isotopic compositions ($\varepsilon_{Nd}(t) = -7.1$ to −7.5, $\varepsilon_{Hf}(t) = -12.3$ to −3.1) with overlapping Nd–Hf model ages of ~1.4–1.6 Ga, indicating derivation from an older meta-igneous crustal source. Potential sources proposed for I-type granites range in composition from basaltic to intermediate rocks (Chappell, 1984, 1999; Rajesh, 2008; Roberts and Clemens, 1993). The PTS and DDA alkali-feldspar granites are characterized by intermediate to high K_2O (4.08–4.81 wt.%) and Na_2O (3.88–4.35 wt.%) concentrations, with K_2O/Na_2O ratios of 0.94–1.21. This is in contrast to the MMEs within the PTS pluton, which have relatively low K_2O (1.44–3.15 wt.%) concentrations and K_2O/Na_2O ratios that generally lie between 0.30 and 0.68 (Zhang et al., 2005). The relatively high K_2O concentrations in these alkali-feldspar granites might have resulted from partial melting of crustal rocks or from plagioclase-dominated fractionation, rather than an input from mantle-derived mafic melts. Granites within both the PTS and DDA plutons have high Rb/Ba and K/Ba ratios, and are significantly depleted in Eu, Ba, and Sr (Fig. 8), all of which suggest that the magmas that formed these rocks fractionated not only plagioclase but also significant amounts of K-feldspar. This indicates that differentiation may not be the dominant process that caused the K_2O enrichments within the northern alkali-feldspar granites. Taken together, these observations suggest that the magma source was the main control on the K-rich nature of the northern I-type granites. The relatively low HFSE and HREE, and relatively high K_2O and Na_2O concentrations within these I-type granites, coupled with their low zircon saturation temperatures (724.7 °C–782.9 °C) and high Rb/Sr ratios, further suggest they were likely derived from a hydrous source in the presence of mica (Chen et al., 2013; King et al., 1997; Sarjoughian et al., 2015).

Studies of experimental dehydration melting have provided evidence of the influence of source rocks on the composition of partial melts and suggests that the partial melting of andesite and several types of low-K metabasalts (K_2O = 0.08–0.82 wt.%) could produce

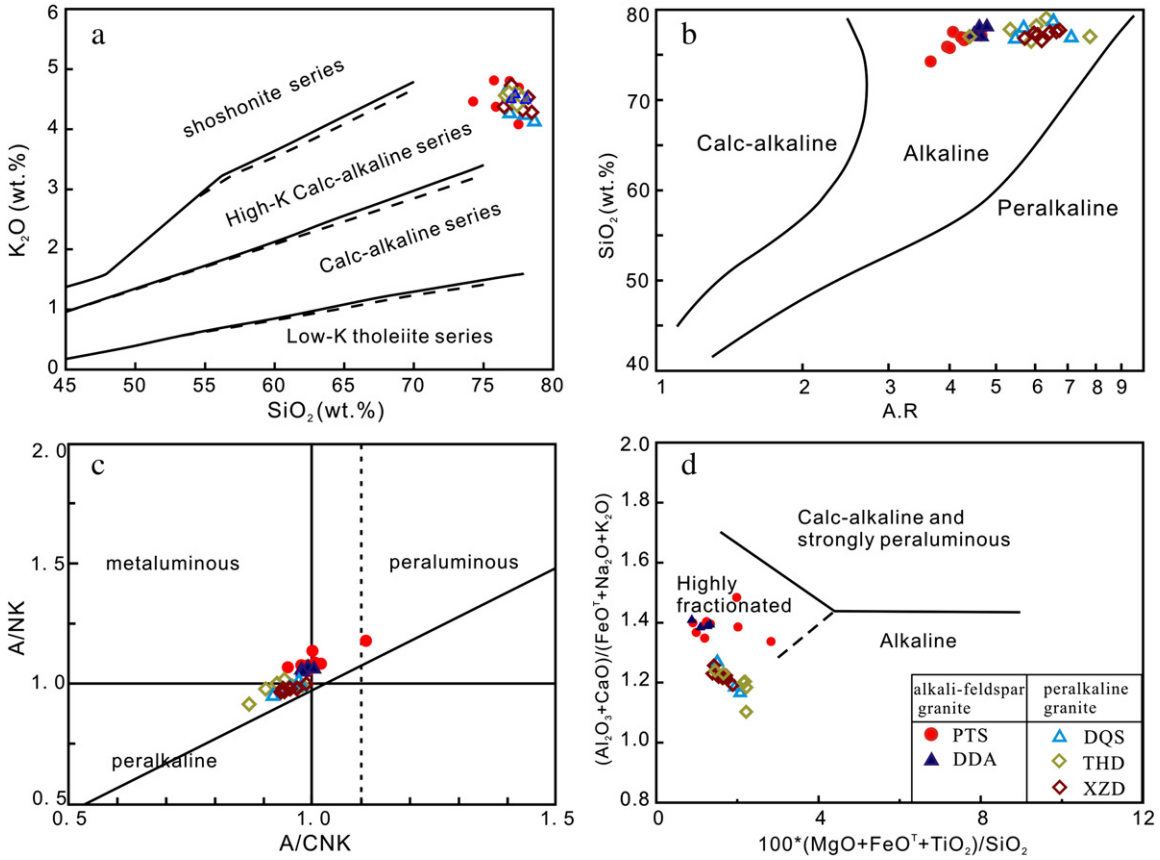

Fig. 7. Chemical classification of granitic rocks from the Zhoushan area, SE China. (a) K_2O vs. SiO_2 diagram (solid lines from Peccerillo and Taylor, 1976; dashed lines from Middlemost, 1985); (b) SiO_2 vs. alkalinity ratio (A.R) diagram (Wright, 1969); (c) A/NK vs. A/CNK diagram (Chappell and White, 1974; Maniar and Piccoli, 1989); (d) $100 \times ((MgO + FeO^T + TiO_2) / SiO_2)$ vs. $(Al_2O_3 + CaO) / (FeO^T + Na_2O + K_2O)$ plot (Sylvester, 1989).

mildly peraluminous to metaluminous granitic melts (Beard and Lofgren, 1991; Rapp and Watson, 1995). However, the melts produced are generally depleted in K_2O and have variable Na_2O and CaO concentrations, all of which contrast with the geochemistry of the PTS and DDA alkali-feldspar granites. Roberts and Clemens (1993) suggested that high-K I-type granitic magmas can only be formed by the partial melting of mafic to intermediate, transitional to high-K calc-alkaline, meta-igneous source rocks. Indeed, previous studies have reported that high-K granitic melts could be generated by the partial melting of tonalitic–granodioritic rocks (Patiño Douce, 1997; Skjerlie and Johnston, 1993). However, such melts are geochemically similar to A-type granites but contrast sharply with the composition of I-type granites. Therefore, the partial melting of intermediate igneous source rocks could not generate the voluminous high-K I-type granites of coastal SE China. Based on an extensive compilation of experimental petrological data, Sisson et al. (2005) ascribed the low-K character of granitic melts to K-poor basaltic starting materials. The authors used medium- to high-K (K_2O = 1.01–2.32 wt.%) basaltic starting material in dehydration melting experiments to produce silicic melts that are slightly peraluminous to metaluminous and contain elevated K_2O and Na_2O concentrations, similar in composition to the PTS and DDA alkali-feldspar granites. Together with their hydrous characteristics, the PTS and DDA alkali-feldspar granites most likely formed from magmas derived from a mica-bearing, K-rich basaltic source.

More recent research has indicated that mantle-derived material plays an important role in the generation of I-type granites, as evidenced by systematic *in situ* U–Pb, Hf, and O isotope analyses of zircons from such granites (He et al., 2010; Kemp et al., 2007; Zhu et al., 2009). The zircons from the northern alkali-feldspar granites have rather variable Hf isotopic compositions, with $\varepsilon_{Hf}(t)$ values of −9.8 to −3.1 and −12.3 to −4.8 for the PTS and DDA granites, respectively (Fig. 9b). These values are different from the signature of magmas derived from a single source with a homogeneous Hf isotopic composition (Griffin et al., 2002; Kemp et al., 2007), indicating the involvement of mantle-derived magma in the generation of the northern alkali-feldspar granites. This hypothesis is supported by the presence of MMEs within the PTS and DDA alkali-feldspar granites. The MMEs are generally spheroidal to ellipsoidal-ovoidal with typical magmatic textures, and they contain K-feldspar xenocrysts from the host alkali-feldspar granite (Fig. 3a). Apatite in the MMEs generally occurs as euhedral acicular crystals (Zhang et al., 2005). The MMEs also contain plagioclase showing reverse compositional zoning (Xie et al., 2004). These petrographic characteristics reflect mixing between mantle-derived mafic and felsic magmas during the generation of these alkali-feldspar granites, providing direct and robust evidence of a magma mixing origin.

Taken together, the field and petrographic observations and geochemical data indicate that the PTS and DDA alkali-feldspar granites formed by the mixing of mantle- and crust-derived magma generated by the dehydration melting of mica-bearing basaltic rocks, combined with further fractionation of plagioclase and K-feldspar during ascent and emplacement.

6.3. Petrogenesis of the A-type DQS, THD, and XZD peralkaline granites

A-type granites are intensively studied because they have unusual geochemical compositions and provide insights into the tectonic setting of ancient terranes. Several petrogenetic models have been proposed for such granites, including: (1) fractional crystallization of mantle-derived basaltic magma (Li et al., 2007; Mushkin et al., 2003; Turner et al., 1992); (2) partial melting of residual source rocks after the extraction of I-type magmas (Clemens et al., 1986; Collins et al., 1982; Whalen et al., 1987); (3) dehydration melting of tonalitic to granodioritic source rocks (Creaser et al., 1991; King et al., 1997; Patiño Douce, 1997); and

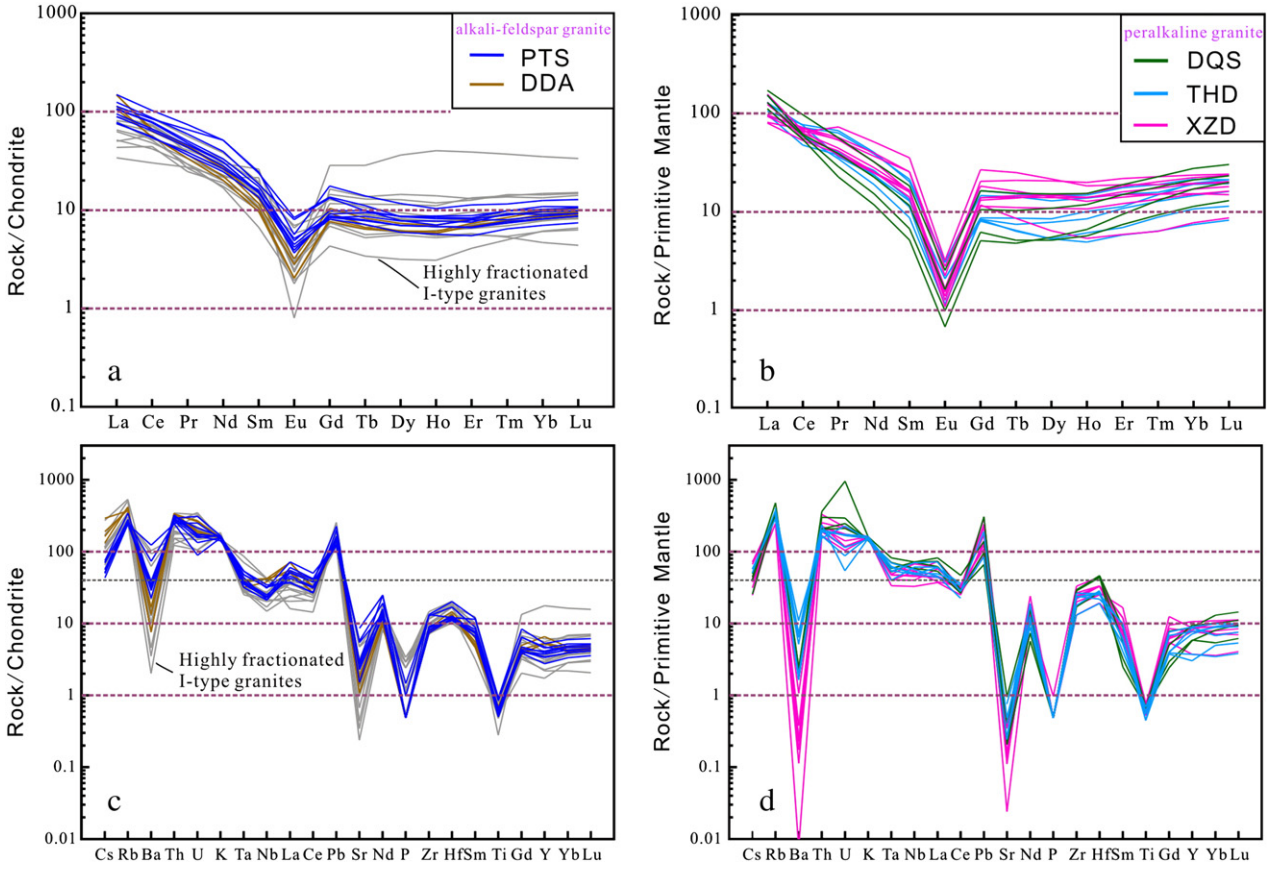

Fig. 8. Chondrite-normalized REE patterns (a, b) and primitive-mantle-normalized trace element spidergrams (c, d) for the Late Cretaceous granites from the Zhoushan area, SE China. The normalization values for chondrite and primitive mantle are from Boynton (1984) and McDonough and Sun (1995), respectively. Data for the highly fractionated I-type granites in the coastal area of SE China are from Qiu et al. (2008) and Zhao et al. (2012).

(4) mixing between anatectic granitic magmas and mantle-derived melts (Barboni and Bussy, 2013; Konopelko et al., 2007). All of the field, petrographic, and geochemical data presented here suggest that the partial melting of granulite-bearing crustal rocks and magma mixing were responsible for the generation of the peralkaline A-type granites in the Zhoushan area.

6.3.1. Magma mixing

Although the origin of A-type granites remains controversial and multiple mechanisms have been proposed for their formation, the role of mantle-derived magmas has been emphasized (Dall'Agnol et al., 2005; Farahat et al., 2007; Huang et al., 2011; Karsli et al., 2012; Konopelko et al., 2007; Qiu et al., 2004; Zhao et al., 2008). The zircons from the southern peralkaline A-type granites have a relatively wide range of Hf isotopic compositions, with $\varepsilon_{Hf}(t)$ values of −7.7 to −3.1 for the DQS pluton, −7.5 to −2.2 for the THD pluton, and −6.3 to −1.6 for the XZD pluton (Fig. 9b). More importantly, these peralkaline granites have more enriched Nd isotopic compositions than the Cretaceous mafic rocks within SE China Coast, and they all plot above the isotope evolution domain for the crustal basement of the South China Block

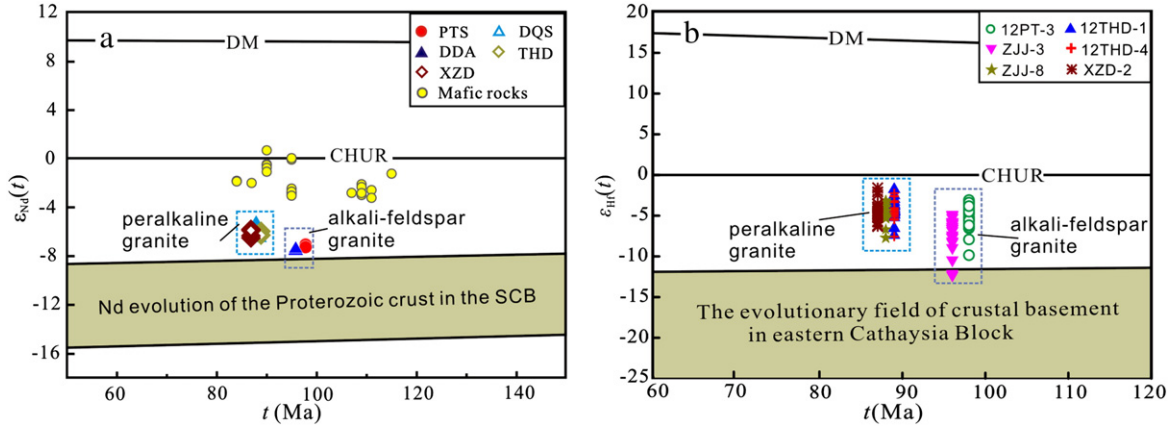

Fig. 9. (a) Age vs. $\varepsilon_{Nd}(t)$ values and (b) Age vs. zircon Hf isotopic compositions for the Late Cretaceous granites from the Zhoushan area, SE China. The Preoterozoic crustal evolutionary field of South China Block (SCB) is after Shen et al. (1993), and the Hf isotopic evolutionary field shown for the crustal basement of the Cathaysia Block is after Xu et al. (2007). Data for the Cretaceous mafic rocks within SE China Coast are from Chen et al. (2013), Li et al. (2014b) and Zhao et al. (2015a) and references therein.

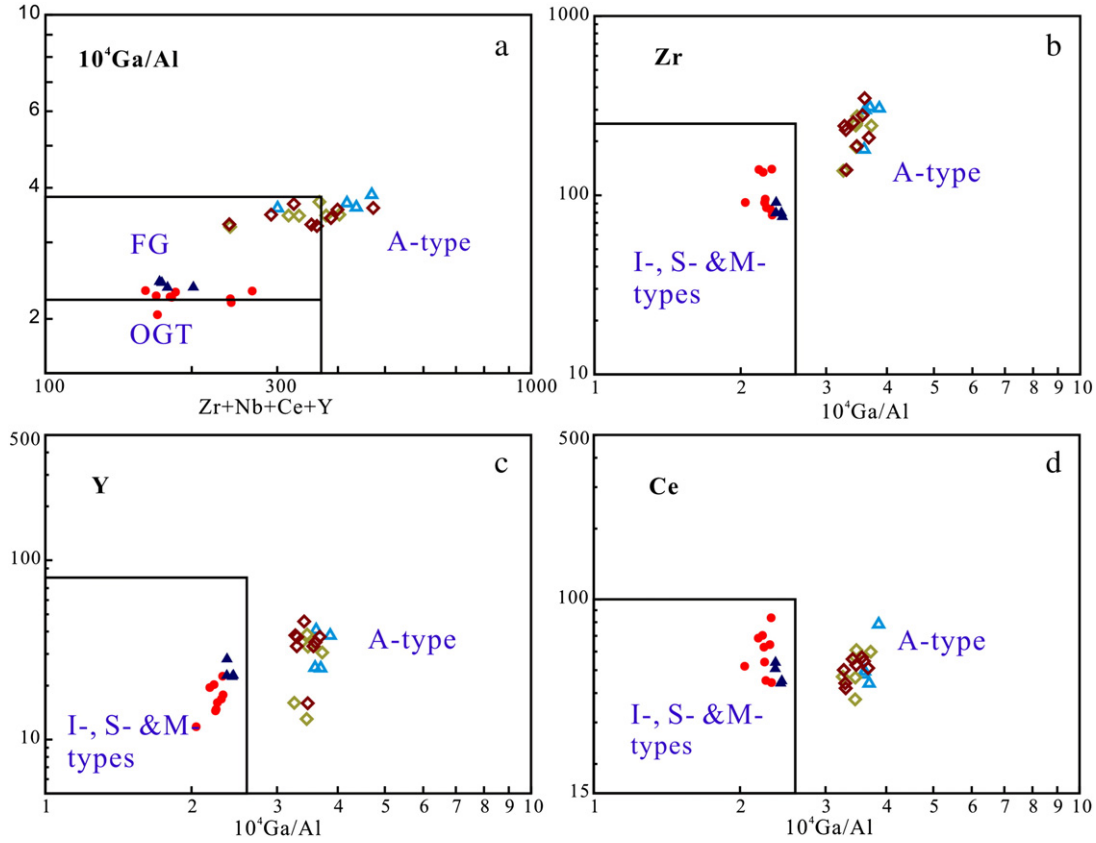

Fig. 10. Plots of (Zr + Nb + Ce + Y) vs. $10^4 \times$ Ga/Al (a) (after Eby, 1990), and $10^4 \times$ Ga/Al vs. Zr (b), Y (c) and Ce (d) (after Whalen et al., 1987), indicating the northern alkali-feldspar granites are affinitive to I-type whereas the southern peralkaline granites are A-type. FG: Fractionated felsic granites; OGT: Unfractionated I-, S-, and M-type granites. Symbols are the same as in Fig. 7.

(Fig. 9a). Consequently, these granites were most likely derived from the remelting of ancient basement rocks with variable inputs of mantle-derived melt. The southern A-type granites have relatively young two-stage Nd and Hf model ages that are inconsistent with any of the known episodes of regional crust generation proposed by Yu et al. (2010) and Xu et al. (2007). This finding also suggests that the DQS, THD, and XZD peralkaline A-type granites are similar to the northern I-type granites in that they formed by the mixing of felsic magmas generated by partial melting of crustal material with depleted mantle-derived magma.

6.3.2. Crustal source signatures

Magmas from crustal and mantle sources contributed to the generation of the DQS, THD, and XZD peralkaline A-type granites, which have negative $\varepsilon_{Nd}(t)$ (−6.5 to −5.7) and $\varepsilon_{Hf}(t)$ (−7.7 to −1.6) values, and high SiO_2 but low FeO^T, MgO, Ni, and Cr concentrations. These granites are A_2-subtype granites (Fig. 11a) according to the scheme of Eby (1992), in which the A_2-subtype granites are thought to be crustal origin. This indicates that crustal material is a major constituent of the southern peralkaline A-type granites.

The southern peralkaline granites are strongly enriched in Nb, Ta, Zr, and Hf, depleted in Ba, Sr, Eu, P, and Ti, and contain high concentrations of F, as is evidenced by the F-enriched arfvedsonite within these granites (3.17–5.06 wt.%). The most striking feature of the DQS, THD and XZD A-type granites is probably their peralkaline character. A key question addressed in this study is whether the parental magmas of these A-type granites were initially peralkaline. Scaillet and Macdonald (2003) suggested that the breakdown of clinopyroxene during melting of a crustal source is likely to produce peralkaline melts. However, Bonin (2007) stressed that no peralkaline A-type parental magmas have been formed experimentally from crustal material. Frost and Frost (2011) suggested that the fractionation of large amount of plagioclase would cause a rapid decrease in Al_2O_3 and CaO concentrations with respect to Na_2O and K_2O in the melt, causing magmas to evolve towards peralkaline compositions. In addition, the wide interval in crystallization temperature (>100 °C) between the plagioclase-saturation boundary and the solidus within A-type magmas, together with the high temperature of this phase boundary, suggests that the prior removal of a large amount of plagioclase would be plausible in A-type magma systems and could therefore cause significant depletions in the CaO concentrations of associated melts (Clemens et al., 1986; Wormald and Price, 1988). The DQS, THD, and XZD peralkaline granites have moderate $K_2O + Na_2O$ concentrations that are indistinguishable from those of the northern metaluminous I-type granites and metaluminous A-type granites within the coastal region of Fujian Province (Fig. 12a). A simple compilation of granite chemical compositions indicates that peralkaline A-type granites generally have higher $K_2O + Na_2O$ concentrations (mainly > 9.0 wt.%) at a given SiO_2 concentration than the rocks within DQS, THD, and XZD plutons (Eyal et al., 2010; Jahn et al., 2009; Litvinovsky et al., 2011; Nardi and Bitencourt, 2009). The peralkaline character of the DQS, THD, and XZD A-type granites is therefore most likely associated with the depleted CaO and Al_2O_3 concentrations within these plutons (Fig. 12b and c), rather than resulting from high Na_2O and K_2O concentrations. This inference is consistent with the rarity or complete lack of plagioclase within these plutons. In addition, the fact that the Ca/Sr and Rb/Sr ratios of the southern peralkaline A-type granites are extremely high and are significantly different from the ratios of the northern I-type granites suggests that the southern peralkaline granites have undergone more extreme plagioclase fractionation than the northern metaluminous I-type granites, even though both sets of granites are highly fractionated and have SiO_2 concentrations >74 wt.%. Therefore, the peralkaline character of

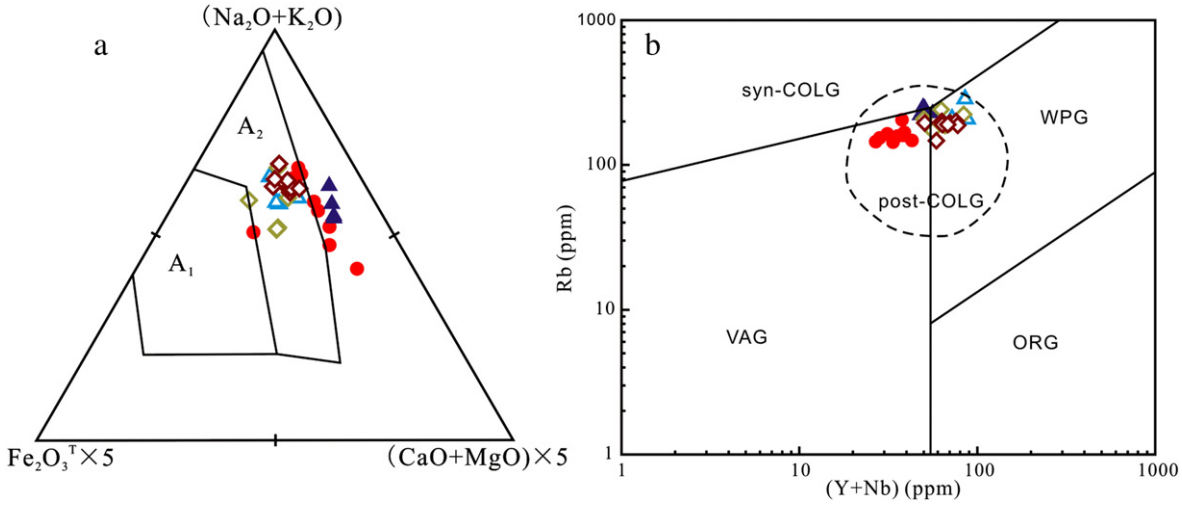

Fig. 11. (a) $(Na_2O + K_2O) - Fe_2O_3^T \times 5 - (CaO + MgO) \times 5$ (mol%) ternary diagram showing the fields for A_1 and A_2 subgroups of A-type plutons (after Grebennikov, 2014); (b) (Y + Nb) vs. Rb diagram of Pearce et al. (1984) showing the field for post-collision granite (post-COLG) from Pearce (1996). Abbreviations: syn-COLG, syn-collision granite; post-COLG, post-collision granite; VAG, volcanic arc granite; WPG, within-plate granite; ORG, ocean ridge granite. The symbols are the same as those in Fig. 7.

the DQS, THD, and XZD A-type granites might be related to the differentiation of metaluminous to slightly peraluminous magmas (especially plagioclase separation) rather than a feature that was inherited from the parental magmas of these granites.

Of note, the two granite types in the present study have a close spatial relationship. Zircon U–Pb age data indicate that the southern DQS, THD and XZD A-type granites postdate the northern PTS and DDA I-type granites by ca. 10 Myr, similarly to other A- and I-type complexes in coastal SE China, such as the Qingtian and the Fuzhou complexes (Dong and Peng, 1994; Lin et al., 2011). In the present case, it is likely that the two granite types have a close genetic relationship. The mica-bearing basaltic rocks, residual granulites, and tonalitic to granodioritic I-type rocks are thus the most plausible source rocks for the southern peralkaline granites. These characteristics, including the concentrated HFSE ratios (e.g., Nb/Ta, Zr/Nb, and Zr/Hf), the presence of significant positive correlations for Ta *vs.* Nb and Zr *vs.* Hf, and the presence of magmatic fluorine-rich minerals (e.g., biotite, arfvedsonite, and fluorite) within the DQS, THD, and XZD A-type granites all suggest that their F-enriched nature was most likely derived from the granitic magma itself rather than from metasomatism by extraneous F-rich fluids (Eby, 1990; Moghazi et al., 2011; Wormald and Price, 1988). King et al. (1997) reported that fractional crystallization could facilitate the enrichment of F in granitic magma. However, it is important to note that the southern peralkaline A-type and the northern I-type granites have nearly indistinguishable SiO_2 contents and D.I. values. The availability of F is therefore another major factor (in addition to magmatic differentiation) that controlled the enrichment of fluorine in the DQS, THD, and XZD granitic magmas. Hence, the granitic rocks in this study were likely derived from different source rocks, and the formation of these peralkaline A-type granites by basaltic source rocks seems unlikely. Moreover, the high magma temperature of the southern peralkaline granites is inconsistent with their generation by the fractionation of I-type parental magma (Clemens et al., 1986; King et al., 2001). In addition, the relatively high concentrations of the HREE and the extreme HFSE enrichments in the southern peralkaline A-type granites argue against their formation from tonalitic to granodioritic source rocks, as metaluminous A-type magmas produced from such sources generally contain low concentrations of both the HREE and the HFSE (e.g., Nb, Ta, and Zr), even within highly evolved magmas (Chen et al., 2013; Farahat et al., 2007; King et al., 1997; Zhao et al., 2015a).

Generally, subsolidus dehydroxylation (OH → F) could increase the stability of biotite and amphibole in the lower crust, and partial melting of such granulitic restite after extraction of granitic melts would generate a relatively anhydrous, F-rich A-type melt (Collins et al., 1982; Whalen et al.,1987). Based on a study of the Chaelundi complex in eastern Australia, Landenberger and Collins (1996) further argued that the residual igneous source could be dehydrated, although generally not refractory/melt-depleted given the occurrence of disequilibrium partial melting. They stressed that once the temperature buffering effect of these dehydration reactions is removed, temperatures would continue to rise to >900 °C, and melting of such granulized source rocks would then proceed and form A-type melts. More recently, Huang et al. (2011) also indicated that A-type granite can be derived from partial melting of granulitic restites under the conditions of asthenospheric upwelling and/or basaltic underplating. Therefore, preference is given to the hypothesis that the southern peralkaline A-type granites were generated from a residual granulitic source.

The DQS, THD, and XZD peralkaline rocks are hypersolvus (i.e., the only feldspar present is alkali feldspar), and hydrous minerals such as biotite and arfvedsonite are generally interstitial, indicating that these peralkaline A-type granites formed from anhydrous magmas (King et al., 1997; Singh and Vallinayagam, 2012; Wormald and Price, 1988). Geochemically, they are strongly enriched in HFSEs, and contain high concentrations of F, HREEs and K_2O, further suggesting their derivation from a residual granulitic source (Chen et al., 2000; Collins et al., 1982; Whalen et al., 1987; Zhao et al., 2008). Thus, the granulite-bearing crustal rocks are the most plausible source for the DQS, THD and XZD peralkaline A-type granites.

In summary, we propose that the southern peralkaline A-type granites were generated by the mixing of mantle-derived material and crustal-derived magmas generated by the partial melting of granulite-bearing source rocks. These magmas then fractionated a significant amount of plagioclase and K-feldspar during ascent and emplacement.

6.4. Petrogenetic model and geodynamic implications

We use a simple binary mixing calculation to further constrain the proportion of mantle and crustal components involved in the formation of the spatially associated peralkaline A- and I-type granites in the Zhoushan area. This calculation used a typical Qilin gabbroic granulite to represent a depleted mantle end-member (Nd = 14 ppm, initial $^{143}Nd/^{144}Nd = 0.512848$; Xu and Zhou, 1995; Xu et al., 1999b) and the average composition of crust in South China to represent a crustal end-member (Nd = 28 ppm, initial $^{143}Nd/^{144}Nd = 0.511810$; Liu et al., 1990). Our calculations indicate that the magmas that formed the northern I-type alkali-feldspar granites can be isotopically modeled

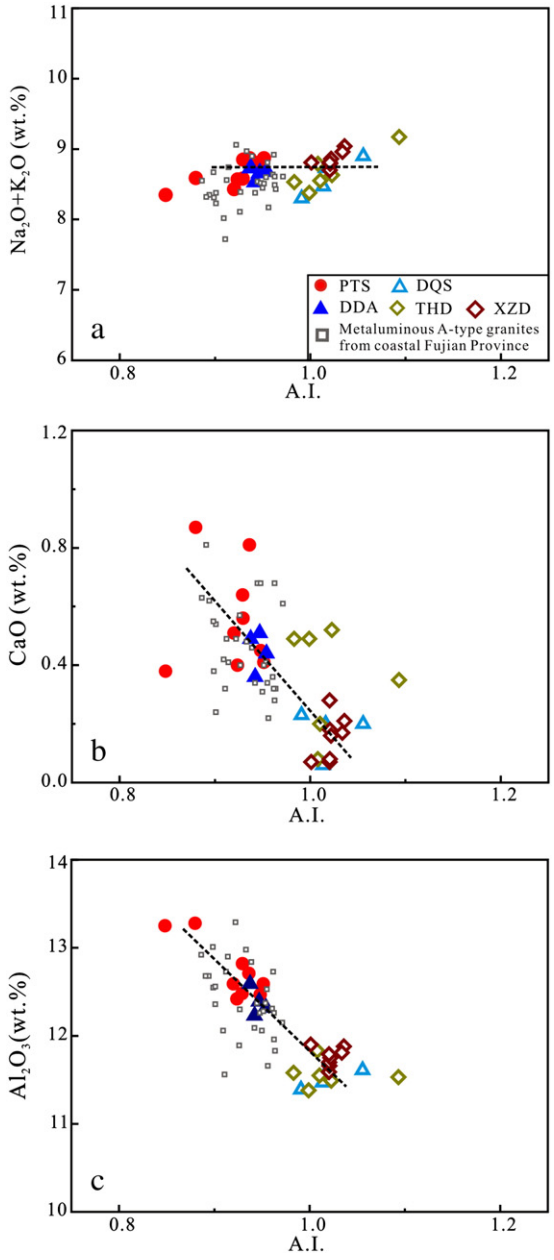

Fig. 12. A.I. (agpaitic index) vs. ($Na_2O + K_2O$), CaO and Al_2O_3 variation diagrams for the studied granites. Data for metaluminous A-type granites in coastal Fujian Province are from Qiu et al. (2004), Chen et al. (2013) and Zhao et al. (2015a).

by mixing ~45% mantle-derived melt with ~55% crustal-derived melt, whereas a slightly higher proportion of mantle-derived melt (~50%) is required to model the compositions of the southern peralkaline A-type granites. Thus, we suggest that the mixing of different proportions of crustal- and mantle-derived magmas, and the presence of closely related but geochemically different source rocks, are the two key factors that controlled the generation of coexisting peralkaline A-type and I-type granites in the Zhoushan area.

An active continental margin setting related to subduction of the palaeo-Pacific plate is widely invoked to explain the Cretaceous igneous magmatism in coastal SE China (Chen et al., 2013; He and Xu, 2012; Martin et al., 1994; Xu et al., 1999a; Zhou et al., 2006). Zircon U–Pb dating indicates that the alkali-feldspar granites and peralkaline granites in the Zhoushan area were emplaced at 98–86 Ma, corresponding to a period of rapid high-angle subduction of the paleo-Pacific plate beneath SE China (Jahn, 1974). He and Xu (2012) suggested that the Cretaceous volcanic–intrusive magmatism in SE China could be grouped into two magmatic episodes: an early stage (140–110 Ma) in a compressional environment, and a late stage (110–85 Ma) in an extensional environment, which were related to the forward and rollback subduction of the paleo-Pacific plate, respectively. Liu et al. (2012) further considered that the change in subduction style might have been related to the "regional magmatic quiescence" at ca. 120–110 Ma, as inferred from a study of the Late Yanshanian lower and upper volcanic series in SE China. However, recent research has identified a series of 120–110 Ma intrusions in the coastal area of SE China, including the Huangtuling gabbro (118 Ma; He and Xu, 2012), the Xiaojiang alkali-feldspar granite (121 Ma) and quartz diorite (114 Ma), and the Longhuangtang alkali-feldspar granites (115 Ma; Wong et al., 2011) in coastal Zhejiang Province, and the Changqiao granodiorite (119 Ma; Qiu et al., 2012) and the Xiaocuo complex (~116 Ma; Li et al., 2015) in coastal Fujian Province. This indicates that the granitic magmatism in the coastal area of SE China was continuous, at least between 125 and 85 Ma.

Eyal et al. (2010) and Liégeois (1998) suggested that post-collisional magmatism is characterized by abundance of high-K calc-alkaline granitoids and terminates with alkaline-peralkaline magmatism. The coastal area of SE China hosts high-K calc-alkaline granitic magmas with crystallization ages of 125–85 Ma (He and Xu, 2012; Li et al., 2014b; Qiu et al., 2008, 2012; Wong et al., 2011; Zhao et al., 2012). The emplacement of A-type granites in this area started slightly later (101 Ma) and lasted till 86 Ma (Zhao et al., 2015a and references therein). Both rock types are thus closely associated in space and time. On the Rb vs. Y + Nb tectonic discrimination diagram (Fig. 11b), data for the granites in this study plot in the post-collision granite (post-COLG) field, suggesting a post-collisional tectonic affinity. In addition, the DQS, THD, and XZD peralkaline A-type granites have an A_2-subtype geochemical affinity, suggesting that these magmas formed in a post-collisional or post-orogenic setting (Eby, 1990, 1992). Therefore, Cretaceous granitic magmatism in the coastal region of SE China most likely occurred in a subduction-related post-collisional continental margin tectonic setting. Wong et al. (2009) investigated the Early Cretaceous Baijuhuajian (125 Ma) and Suzhou (123 Ma) granites (Fig. 1), classifying them as A-type granitic plutons and indicating that extension in SE China started at 125 Ma at the latest, earlier than previously suggested (110 Ma). In addition, numerous extension-related rocks, such as A-type granites, bimodal volcanic rock associations, and basic dikes, are widespread throughout coastal SE China. The magmatism that formed these rocks occurred over a short period (101–83 Ma; Zhao et al., 2015a and references therein), indicating a Late Cretaceous peak in regional lithospheric extension caused by rollback of the subducting paleo-Pacific plate. The presence of well-developed miarolitic cavities and granophyric texture in these A-type granites, even in some of the coeval I-type granites (Qiu et al., 2008), is indicative of high-level emplacement and also provides evidence for an extensional regime (Chen et al., 2004). Taken together, the petrological, geochemical, and geochronological data for Cretaceous granites in coastal SE China indicate that the granitic magmatism in the Zhoushan area occurred in a post-collisional extensional setting, with the intensity of regional tectonic extension increasing between the Early and Late Cretaceous.

Here, we suggest a simplified genetic model for the closely associated I-type alkali-feldspar granites and A-type peralkaline granites in the Zhoushan area (Fig. 13). This model involves early regional extension (~125 Ma) that induced underplating of mantle-derived magmas and the subsequent partial melting of lower crustal rocks, producing felsic magmas. These crustal melts then mixed with the underplated basaltic magmas, forming the parental magmas that eventually produced the calc-alkaline I-type granites in the Zhoushan area (Fig. 13a). This also caused the simultaneous formation of residual granulitic rocks within the lower crust. The later stages of Cretaceous magmatism (Fig. 13b) were associated with an increase in the dip angle of the subducting slab and oceanward retreat of the trench, causing an increase in

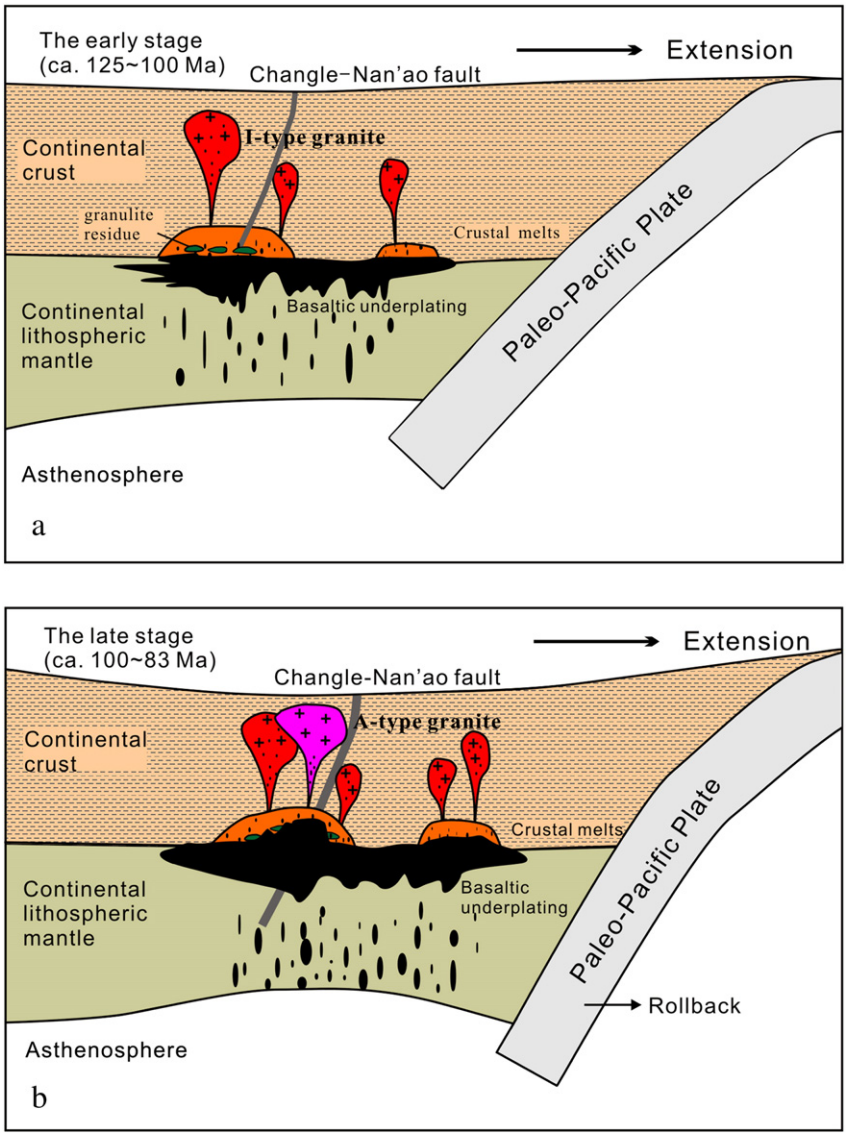

Fig. 13. Cartoon illustrating a petrogenetic model for generation of I- and A-type granites in the coastal area of SE China. (a) underplating of mantle-derived magma induced partial melting of crustal materials to produce felsic magma, leaving granulite residues in the lower crust. The felsic magma then mixed with mantle-derived melts, forming the parental magma of the PTS and DDA I-type granites. (b) With ongoing increase of the dip angle of the subducted palaeo-Pacific plate in Cretaceous, the degree of lithosphere extension gradually intensified, and induced the activation of Changle–Nan'ao Fault. The accompanying large-scale mantle-derived magma underplating resulted in melting of the residual granulitic rocks to form crust-derived F-bearing melts, and subsequent mixing between mantle- and crust- derived melts finally produced the parental magma of the southern peralkaline A-type granites. After further but different magma evolution processes, both types of remaining melts emplaced along the Changle–Nan'ao fault, and finally formed the spatially coexisting calc-alkaline I-type and peralkaline A-type granites in the Zhoushan area.

extension, further thinning the lithosphere and inducing more intensive underplating of mantle-derived magmas along the Changle–Nan'ao Fault. This generated high temperatures within the crust and caused partial melting of the residual granulitic material, producing relatively anhydrous F-containing felsic melts. Mixing of these unusual crustal melts with larger volumes of mantle-derived mafic magmas generated the parental magmas that eventually formed the peralkaline A-type granites. The I- and A-type parental magmas subsequently underwent further differentiation involving variable fractional crystallization paths during their emplacement along the Changle–Nan'ao Fault, and finally formed the spatially coexisting calc-alkaline I-type and peralkaline A-type granites in the Zhoushan area.

7. Conclusions

(1) The PTS and DDA alkali-feldspar granites (98–96 Ma), and the DQS, THD, and XZD peralkaline granites (89–86 Ma) were emplaced from north to south during the later stages of Cretaceous magmatism within the Zhoushan archipelago, in the coastal region of Zhejiang Province.

(2) The northern alkali-feldspar granites are high-K calc-alkaline, metaluminous to mildly peraluminous, contain magnesian biotite and calcic amphibole, and have low Ga/Al ratios, all of which are indicative of an I-type affinity. In contrast, the southern granites are peralkaline, enriched in the HFSE, and have elevated Ga/Al ratios, indicative of an A-type affinity.

(3) The northern I-type alkali-feldspar granites were formed by the mixing of mantle- and crust-derived magma generated by the dehydration melting of mica-bearing basaltic rocks, whereas the southern peralkaline A-type granites were produced by the mixing of mantle-derived material and crustal-derived magmas generated by the partial melting of residual granulitic source. A combination of factors, including variations in the mixing ratio between crustal- and mantle-derived magmas and geochemical differences

between source rocks, most likely led to the generation of coexisting I- and A-type granites within the Zhoushan area.

(4) Both the I- and A-type granites formed in a post-collisional extensional tectonic setting as a result of high-angle rollback of the subducting paleo-Pacific plate. Cretaceous continuous tectonic extension, underplating of mantle-derived magmas, and reactivation of the Changle–Nan'ao Fault during subduction may all have contributed to the voluminous granite magmatism in coastal SE China.

Acknowledgments

We are indebted to Prof. Jin-Cheng Zhou for his help in preparation the early draft of this manuscript. We also thank Editor-in-Chief Dr. Andrew Kerr and two anonymous reviewers for their thoughtful comments and constructive suggestions which greatly improved the manuscript. This study was financially supported by the National 973 Project of the Chinese Ministry of Science and Technology (grant no. 2012CB416702), and the Specialized Research Fund for the Doctoral Program of Higher Education of China (grant no. 20120091130003).

Appendix A. Supplementary data

Supplementary data to this article can be found online at http://dx.doi.org/10.1016/j.lithos.2015.10.018.

References

Andersen, T., 2002. Correction of common lead in U–Pb analyses that do not report ^{204}Pb. Chemical Geology 192, 59–79.
Barbarin, B., 1999. A review of the relationships between granitoids types, their origins and their geodynamic environments. Lithos 46, 605–626.
Barboni, M., Bussy, F., 2013. Petrogenesis of magmatic albite granites associated to cogenetic A-type granites: Na-rich residual melt extraction from a partially crystallized A-type granite mush. Lithos 177, 328–351.
Beard, J.S., Lofgren, G.E., 1991. Dehydration melting and water-saturated melting of basaltic and andesitic greenstones and amphibolites at 1, 3, and 6.9 kb. Journal of Petrology 32, 365–401.
Black, L.P., Gulson, B.L., 1978. The age of the mud tank carbonatite, Strangways range, Northern territory. BMR Journal of Australian Geology and Geophysics 3, 227–232.
Bonin, B., 2007. A-type granites and related rocks: evolution of a concept, problems and prospects. Lithos 97 (1–2), 1–2.
Boynton, W.V., 1984. Geochemistry of the rare earth elements: meteorite studies. In: Henderson, P. (Ed.), Rare Earth Elements Geochemistry. Elservier, Amsterdam, pp. 63–144.
Breiter, K., 2012. Nearly contemporaneous evolution of the A- and S-type fractionated granites in the Krušné hory/Erzgebirge Mts., Central Europe. Lithos 151, 105–121.
Chappell, B.W., 1984. Source rocks of S- and I-type granites in the Lachlan Fold Belt, southeastern Australia. Philosophical Transactions of the Royal Society of London A310, 693–707.
Chappell, B.W., 1999. Aluminium saturation in I- and S-type granites and the characterization of fractionated haplogranites. Lithos 46, 535–551.
Chappell, B.W., White, A.J.R., 1974. Two contrasting granite types. Pacific Geology 8, 173–174.
Chen, J.F., Jahn, B., 1998. Crustal evolution of southeastern China: Nd and Sr isotopic evidence. Tectonophysics 284, 101–133.
Chen, C.H., Lin, W., Lee, C.Y., Tien, J.L., Lu, H.Y., Lai, Y.H., 2000. Cretaceous fractionated I–type granitoids and metaluminous A-type granites in SE China: the Late Yanshanian post-orogenic magmatism. Transaction Royal Society of Edinburgh: Earth Science 91, 195–205.
Chen, C.H., Lin, W., Lan, C.Y., Lee, C.Y., 2004. Geochemical and Sr, Nd isotopic characteristics and tectonic implications for three stages of igneous rock in the Late Yanshanian (Cretaceous) orogeny, SE China. Transaction Royal Society of Edinburgh: Earth Science 95, 237–248.
Chen, J.Y., Yang, J.H., Zhang, J.H., Sun, J.F., Wilde, S.A., 2013. Petrogenesis of the Cretaceous Zhangzhou batholith in southeastern China: zircon U-Pb age and Sr-Nd-Hf-O isotopic evidence. Lithos 162–163, 140–156.
Clemens, J.D., 2003. S-type granitic magmas–petrogenetic issues, models and evidence. Earth Science Reviews 61 (1–2), 1–18.
Clemens, J.D., Holloway, J.R., White, A., 1986. Origin of an A-type granite: experimental constraints. American Mineralogist 71, 317–324.
Collins, W.J., Beams, S.D., White, A.J.R., Chappell, B.W., 1982. Nature and origin of A-type granites with particular reference to southeastern Australia. Contrib Mineral Petrology 80, 189–200.
Creaser, R.A., Price, R.C., Wormald, R.J., 1991. A-type granites revisited: assessment of a residual-source modal. Geology 19, 163–166.
Dall'Agnol, R., Teixeira, N.P., Rämö, O.T., Moura, c.a., Macambira, M.J.B., Oliveira, D.C., 2005. Petrogenesis of the Paleoproterozoic, rapakivi, A-type granites of the Archean Carajás Metallogenic Province, Brazil. Lithos 80, 101–129.
Dong, C.W., Peng, Y.M., 1994. Qingtian composite body—the coexisting of two different types of granites. Journal of Zhejiang University: Nature Science 28 (4), 440–448 (in Chinese with English abstract).
Eby, G.N., 1990. A-type granitoids: a review of their occurrence and chemical characteristics and speculations on their petrogenesis. Lithos 26, 115–134.
Eby, G.N., 1992. Chemical subdivision of the A-type granitoids: petrogenetic and tectonic implications. Geology 20, 641–644.
Eyal, E., Litvinovsky, B., John, B.M., Zanvilevich, A., Katzir, Y., 2010. Origin and evolution of post–collisional magmatism: Coeval Neoproterozoic calc-alkaline and alkaline suites of the Sinai Peninsula. Chemical Geology 269, 153–179.
Farahat, E.S., Mohamed, H.A., Ahmed, A.F., Mahallawi, M.M.E., 2007. Origin of I- and A-type granitoids from the Eastern Desert of Egypt: Implications for crustal growth in the northern Arabian-Nubian Shield. Journal of African Earth Sciences 49, 43–58.
Frost, C.D., Frost, B.R., 2011. On ferroan (A-type) granitoids: their compositional variability and modes of origin. Journal of Petrology 52 (1), 39–53.
Gao, J.F., Lu, J.J., Lin, Y.P., Pu, W., 2003. Analysis of trace elements in rock samples using HR-ICPMS. Journal of Nanjing University (Natural Sciences) 39, 844–850 (in Chinese with English abstract).
Ghani, A.A., Searle, M., Robb, L., Chung, S.L., 2013. Transitional I S type characteristic in the Main Range Granite, Peninsular Malaysia. Journal of Asian Earth Sciences 76, 225–240.
Goodge, J.W., Vervoort, J.D., 2006. Origin of Mesoproterozoic A-type granites in Laurentia: Hf isotope evidence. Earth and Planetary Science Letters 243, 711–731.
Grebennikov, A.V., 2014. A-type granites and related rocks: petrogenesis and classification. Russian Geology and Geophysics 55, 1074–1086.
Griffin, W.L., Wang, X., Jackson, S.E., Pearson, N.J., O'Reilly, S.Y., Xu, X.S., Zhou, X.M., 2002. Zircon chemistry and magma mixing, SE China: in-situ analysis of Hf isotopes, Tonglu and Pingtan igneous complexes. Lithos 61, 237–269.
Griffin, W.L., Pearson, N.J., Belousova, E.A., 2007. Reply to "Comment to short-communication 'Comment: Hf –isotope heterogeneity in zircon 91500' by W.L. Griffin, N.J. Pearson, E.A. Belousova and A. Saeed (Chemical geology 233 (2006) 358-363) " by F. Corfu. Chemical Geology 244 (1–2), 354–356.
He, Z.Y., Xu, X.S., 2012. Petrogenesis of the late Yanshanian mantle-derived intrusions in southeastern China: response to the geodynamics of paleo-Pacific plate subduction. Chemical Geology 328, 208–221.
He, Z.Y., Xu, X.S., Niu, Y.L., 2010. Petrogenesis and tectonic significance of a Mesozoic granite-syenite-gabbro association from inland South China. Lithos 119, 621–641.
Heilimo, E., Elburg, M.A., Andersen, T., 2014. Crustal growth and reworking during Lapland–Kola orogeny in northern Fennoscandia: U–Pb and Lu–Hf data from the Nattanen and Litsa–Aragub–type granites. Lithos 205, 112–126.
Huang, H.Q., Li, X.H., Li, W.X., Li, Z.X., 2011. Formation of high δ^{18}O fayalite-bearing A-type granite by high-temperature melting of granulitic metasedimentary rocks, southern China. Geology 39, 903–906.
Jackson, S.E., Pearson, N.J., Griffin, W.L., Belousoval, E.A., 2004. The application of laser ablation-inductively coupled plasma-mass spectrometry (LA-ICP-MS) to in situ U-Pb zircon geochronology. Chemical Geology 211, 47–69.
Jahn, B.M., 1974. Mesozoic thermal events in southeast China. Nature 248, 480–483.
Jahn, B.M., Litvinovsky, B.A., Zanvilevich, A.N., Reichow, M., 2009. Peralkaline granitoid magmatism in the Mongolian–Transbaikalian Belt: Evolution, petrogenesis and tectonic significance. Lithos 113, 521–539.
Jiang, Y.H., Zhao, P., Zhou, Q., Liao, S.Y., Jin, G.D., 2011. Petrogenesis and tectonic implications of Early Cretaceous S-and A-type granites in the northwest of the Gan-Hang rift, SE China. Lithos 121, 55–73.
Karsli, O., Caran, Ş., Dokuz, A., Çoban, H., Chen, B., Kandermir, R., 2012. A-type granitoids from the Eastern Pontides, NE Turkey: Records for generation of hybrid A-type rocks in a subduction-related environment. Tectonophysics 530–531, 208–224.
Kemp, A., Hawkesworth, C., 2003. Granitic perspective on the generation and secular evolution of the continental crust. Treatise on Geochemistry. Elsevier Ltd, pp. 349–410.
Kemp, A., Hawkesworth, C.J., Froster, G.L., Paterson, B.A., Wooodhead, J.D., Hergt, J.M., Gray, C.M., Whitehose, M.J., 2007. Magmatic and crustal differentiation history of granitic rocks from Hf–O isotopes in zircon. Science 315 (5814), 980–983.
King, P.L., White, A.J.R., Chappell, B.W., Allen, C.M., 1997. Characterization and origin of aluminous A-type granites from the Lachlan Fold Belt, Southeastern Australia. Journal of Petrology 38 (3), 371–391.
King, P.L., Chappell, B.W., Allen, C.M., White, A.J.R., 2001. Are A-type granites the high-temperature felsic granites? Evidence from fractionated granites of the Wangrah Suite. Australian Journal of Earth Sciences 48, 501–514.
Konopelko, D., Biske, G., Seltmann, R., Eklund, O., Belyatsky, B., 2007. Hercynian post-collisional A-type granites of the Kokshaal Range, Southern Tien Shan, Kyrgyzstan. Lithos 97, 140–160.
Landenberger, B., Collins, W.J., 1996. Derivation of A-type granites from a dehydrated charnockitic lower crust: Evidence from the Chaelundi Complex, eastern Australia. Journal of Petrology 37, 145–170.
Leake, B.E., Woolley, A.R., Arps, C.E.S., Birch, W.D., Gilbert, M.C., Grice, J.D., Hawthorne, F.C., Kato, A., Kisch, H.J., Krivovichev, V.G., Linthout, K., Laird, J., Mandarino, J., Maresch, W.V., Nickel, E.H., Schumacher, J.C., Smith, D.C., Stephenson, N.C.N., Ungaretti, L., Whittaker, E.J.W., Youzhi, G., 1997. Nomenclature of amphiboles: Report of the Subcommittee on Amphiboles of the International Mineralogical Association, Commission on New Minerals and Mineral names. The Canadian Mineralogist 35, 219–246.
Li, X.H., Li, Z.X., Li, W.X., Liu, Y., Yuan, C., Wei, G.J., Qi, C.S., 2007. U–Pb zircon, geochemical and Sr-Nd-Hf isotopic constraints on age and origin of Jurassic I- and A-type granites from central Guangdong, SE China: A major igneous event in response to foundering of a subducted flat-slab? Lithos 96 (1–2), 186–204.

Li, X.H., Li, Z.X., Li, W.X., 2014a. Detrital zircon U–Pb age and Hf isotope constrains on the generation and reworking of Precambrian continental crust in the Cathaysia Block, South China: A synthesis. Gondwana Research 25, 1202–1215.
Li, Z., Qiu, J.S., Yang, X.M., 2014b. A review of the geochronology and geochemistry of Late Yanshanian (Cretaceous) plutons along the Fujian coastal area of southeastern China: Implications for magma evolution related to slab break-off and rollback in the Cretaceous. Earth Science Review 128, 232–248.
Li, Y., Ma, C.Q., Xing, G.F., Zhou, H.W., Zhang, H., Brouwer, F.M., 2015. Origin of a Cretaceous low-^{18}O granitoids complex in the active continental margin of SE China. Lithos 216–217 (2015), 136–147.
Liégeois, J.P., 1998. Preface– some words on the post-collisional magmatism. Lithos 45, 15–17.
Lin, Q.C., Cheng, X.W., Zhang, Y.Q., Wang, F.Y., 2011. Evolution of granitoids in the active continental margin: a case study of the Fuzhou compound complex. Acta Geologica Sinica 85 (7), 1128–1133 (in Chinese with English abstract).
Litvinovsky, B.A., Tsygankov, A.A., Jahn, B.M., Katzir, Y., Be'eri-Shlevin, Y., 2011. Origin and evolution of overlapping calc-alkaline and alkaline magmas: The Late Palaeozoic post-collisional igneous province of Transbaikalia (Russia). Lithos 125, 845–874.
Liu, C.S., Zhu, J.C., Shen, W.Z., Xu, S.J., 1990. Evolution of continental crust and material source (genesis) of granitoids in south China. Geotectonica et Metallogenia 14, 125–138 (in Chinese with English abstract).
Liu, L., Xu, X.S., Zou, H.B., 2012. Episodic eruptions of the late Mesozoic volcanic sequences in southeastern Zhejiang, SE China: petrogenesis and implications for the geodynamics of paleo-Pacific subduction. Lithos 154, 166–180.
Loiselle, M.C., Wones, D.R., 1979. Characteristics and origin of anorogenic granites. Abstracts papers to be presented at the Annual Meetings of the Geological Society of America and Associated Societies, San Diego, CA 11, 468.
Ludwig, K.R., 2001. Isoplot/Ex (rev. 2.49): a geochronological toolkit for Microsoft Excel: Berkeley Geochronology Center. Special Publication 1, 1–58.
Maniar, P.D., Piccoli, P.M., 1989. Tectonic discrimination of granitoids. Geological Society of America Bulletin 101, 635–643.
Martin, H., Bonin, B., Capdevila, R., Jahn, B.M., Lameyre, J., Wang, Y., 1994. The Kuiqi peralkaline granitic complex (SE China): petrology and geochemistry. Journal of Petrology 35, 983–1015.
McDonough, W.F., Sun, S.S., 1995. The composition of the Earth. Chemical Geology 120, 223–253.
Middlemost, E.A.K., 1985. Magma and Magmatic Rocks. Longman, London (266 pp.).
Moghazi, A.M., Harbi, H.M., Ali, K.A., 2011. Geochemistry of the Late Neoproterozoic Hadb adh Dayheen ring complex, Central Arabian Shield: Implications for the origin of rare–metal-bearing post-orogenic A-type granites. Journal of Asian Earth Sciences 42, 1324–1340.
Morimoto, N., Fabries, J., Ferguson, A.K., Ginzburg, I.V., Ross, M., Seifert, F.A., Zussman, J., Aoki, K., Gottard, G., 1988. Nomenclature of Pyroxenes. Mineralogy and Petrology 39, 55–76.
Mushkin, A., Navon, O., Halicz, L., Hartmann, G., Stein, M., 2003. The petrogenesis of A-type magmas from the Amram Massif, southern Israel. Journal of Petrology 44, 815–832.
Nardi, L.V.S., Bitencourt, M.F., 2009. A-type granitic rocks in post-collisional settings in southernmost Brazil: Their classification and relationship with tectonics and magmatic series. The Canadian Mineralogist 47, 1493–1503.
Patiño Douce, A.E., 1997. Generation of metaluminous A-type granitoids by low-pressure melting of calc-alkaline granitoids. Geology 25, 743–746.
Pearce, J.A., 1996. Sources and settings of granitic rocks. Episodes 19, 120–125.
Pearce, J.A., Harris, N.B.W., Tindle, A.G., 1984. Trace element discrimination diagrams for the tectonic interpretation of granitic rocks. Journal of Petrology 25, 956–983.
Peccerillo, A., Taylor, D.R., 1976. Geochemistry of Eocene calc-alkaline volcanic rocks from the Kaitamonu area, Northern Turkey. Contributions to Mineralogy and Petrology 58, 63–91.
Pu, W., Zhao, K.D., Ling, H.F., Jiang, S.Y., 2004. High precision Nd isotopes measurement by Triton TI Mass Spectrometry. Acta Geoscientica Sinica 25, 271–274 (in Chinese with English abstract).
Pu, W., Gao, J.F., Zhao, K.D., Lin, H.F., Jiang, S.Y., 2005. Separation method of Rb-Sr, Sm-Nd using DCTA and HIBA. Journal of Nanjing University (Nature Sciences) 41, 445–450 (in Chinese with English abstract).
Qiu, J.S., Wang, D.Z., Mclnnes, B.I.A., 1999. Geochemistry and petrogenesis of the I- and A-type composite granite masses in the coastal area of Zhejiang and Fujian Provinces. Acta Petrologica Sinica 15 (2), 237–246 (in Chinese with English abstract).
Qiu, J.S., Wang, D.Z., Mclnnes, B.I.A., Jiang, S.Y., Wang, R.C., Kanisawa, S., 2004. Two subgroups of A-type granites in the coastal area of Zhejiang and Fujian Provinces, SE China: age and geochemical constraints on their petrogenesis. Transactions of the Royal Society of Edinburgh: Earth Sciences 95, 227–236.
Qiu, J.S., Xiao, E., Hu, J., Xu, X.S., Jiang, S.Y., Li, Z., 2008. Petrogenesis of highly fractionated I–type granites in the coastal area of northeastern Fujian Province: Constraints from zircon U-Pb geochronology, geochemistry and Nd-Hf isotopes. Acta Petrologica Sinica 24 (11), 2468–2484 (in Chinese with English abstract).
Qiu, J.S., Li, Z., Liu, L., Zhao, J.L., 2012. Petrogenesis of the Zhangpu composite granite pluton in Fujian Province: constraints from zircon U-Pb ages, elements geochemistry and Nd-Hf isotopes. Acta Geologica Sinica 86 (4), 561–576 (in Chinese with English abstract).
Rajesh, H.M., 2008. Petrogenesis of two granites from the Nilgiri and Madurai blocks, southwestern India: Implications for charnockite-calc-alkaline granite and charnockite-alkali (A-type) granite link in high-grade terrains. Precambrian Research 162, 180–197.
Rapp, R.P., Watson, E.B., 1995. Dehydration melting of metabasalt at 8–32 kbar: implications for continental growth and crust–mantle recycling. Journal of Petrology 36, 891–931.
Roberts, M.P., Clemens, J.D., 1993. Origin of high-potassium, calc-alkaline, I-type granitoids. Geology 21, 825–828.
Sarjoughian, F., Kananian, A., Haschke, M., Ahmadian, J., 2015. Transition from I-type to A-type magmatism in the Sanandaj-Sirjan Zone, NW Iran: an extensional intracontinental arc. Geological Journal http://dx.doi.org/10.1022/gj.2637.
Scaillet, B., Macdonald, R., 2003. Experimental constraints on the relationships between peralkaline rhyolites of the Kenya Rift Valley. Journal of Petrology 44 (10), 1867–1894.
Shen, W.Z., Zhu, J.C., Liu, C.S., Xu, S.J., Ling, H.F., 1993. Sm-Nd isotopic study of basement metamorphic rocks in south China and its constraint on material sources of granitoids. Acta Petrologica Sinica 9, 115–124 (in Chinese).
Singh, L.G., Vallinayagam, G., 2012. Petrological and geochemical constraints in the origin and associated mineralization of A-type granite suite of the Dhiran Area, northwestern Peninsular India. Geosciences 2 (4), 66–80.
Sisson, T., Ratajeski, K., Hankins, W., Glazner, A., 2005. Voluminous granitic magmas from common basaltic sources. Contributions to Mineralogy and Petrology 148, 635–661.
Skjerlie, K.P., Johnston, A.D., 1993. Fluid-absent melting behavior of an F-rich tonalitic genesis at mid-crustal pressures: Implications for the generation of anorogenic granites. Journal of Petrology 34, 785–815.
Sylvester, P.J., 1989. Post–collisional alkaline granites. The Journal of Geology 97 (3), 261–280.
Turner, S.P., Foden, J.D., Morrison, R.S., 1992. Derivation of some A-type magmas by fractionation of basaltic magma: an example from the Padthaway Ridge, South Australia. Lithos 28, 151–179.
Van Achterbergh, E., Ryan, C.G., Jackson, S.E., Griffin, W.L., 2001. Data reduction software for LA-ICP-MS: appendix. In: Sylvester, P.J. (Ed.), Laser Ablation-ICP-Mass Spectrometry in the Earth Sciences: Principles and Applications, Mineralogical Association of Canada (MAC) Short Course Series, Ottawa, Ontario, Canada. 29, pp. 239–243.
Whalen, J.B., Currie, K.L., Chappell, B.W., 1987. A-type granites: geochemical characteristics, discrimination and petrogenesis. Contributions to Mineralogy and Petrology 95 (4), 407–419.
Wong, J., Sun, M., Xing, G.F., Li, X.H., Zhao, G.C., Wong, K., Yuan, C., Xia, X.P., Li, L.M., Wu, F.Y., 2009. Geochemical and zircon U-Pb and Hf isotopic study of the Baijuhuajian metaluminous A-type granite: Extension at 125-100 Ma and its tectonic significance for South China. Lithos 112, 289–305.
Wong, J., Sun, M., Xing, G.F., Li, X.H., Zhao, G.C., Wong, K., Wu, F.Y., 2011. Zircon U-Pb and Hf isotopic study of Mesozoic felsic rocks from eastern Zhejiang, South China: Geochemical contrast between the Yangtze and Cathaysia blocks. Gondwana Research 19, 244–259.
Wormald, R.J., Price, R.C., 1988. Peralkaline granites near Temora, southern New South Wales: Tectonic and petrological implications. Australian Journal of Earth Sciences 35, 209–221.
Wright, J.B., 1969. A simple alkalinity ratio and its application to questions of nonorogenic granite genesis. Geological Magazine 106 (4), 370–384.
Xie, X.J., Yan, M.C., Wang, C.S., Li, L.Z., Shen, H.J., 1989. Geochemical standard reference samples GSD 9-12, GSS 1-8 and GSR 1-6. Geostandards and Geoanalytical Research 13, 83–179.
Xie, L., Wang, D.Z., Wang, R.C., Qiu, J.S., Chen, X.M., 2004. Complex zoning texture in plagioclase from the quartz diorite enclave in the Putuo granitc complex, Zhejiang Province: record of magma mixing. Acta Petrologica Sinica 20 (6), 1397–1408 (in Chinese with English abstract).
Xu, X.S., Zhou, X.M., 1995. The xenoliths from Qilin Cenozoic basaltic pipe, Guangdong. Acta Petrologica Sinica 11 (4), 441–448 (in Chinese with English abstract).
Xu, X.S., Dong, C.W., Li, W.X., Zhou, X.M., 1999a. Late Mesozoic intrusive complexes in the coastal area of Fujian SE China: the significance of the gabbro-diorite-granite association. Lithos 46, 299–315.
Xu, X.S., Zhou, X.M., O'Reolly, S.Y., Tang, H.F., 1999b. Exploration for the lower crustal materials and granite genesis in southeast China. Acta Petrologica Sinica 15 (2), 217–223 (in Chinese with English abstract).
Xu, X.S., O'Reilly, S.Y., Griffin, W.L., Pearson, N.J., He, Z.Y., 2007. The crust of Cathaysia: age, assembly and reworking of two terranes. Precambrian Research 158, 51–78.
Yu, J.H., O'Reilly, S.Y., Suzanne, Y., Wang, L.J., Griffin, W.L., Zhou, M.F., Zhang, M., Shu, L.S., 2010. Components and episodic growth of Precambrian crust in the Cathaysia Block, South China: Evidence from U–Pb ages and Hf isotopes of zircons in Neoproterozoic sediments. Precambrian Research 181 (1–4), 97–114.
Zhang, Z.J., Wang, Y.H., 2007. Crustal structure and contact relationship revealed from deep seismic sounding data in South China. Physics of the Earth and Planetary Interiors 165, 114–126.
Zhang, X.L., Qiu, J.S., Wang, D.Z., Wang, R.C., Xu, X.S., Chen, X.M., 2005. Geochemistry and magmatic mixing of the Putuoshan biotite moyites and their enclaves, Zhejiang Province. Acta Petrologica et Mineralogica 24 (2), 81–92 (in Chinese with English abstract).
Zhao, X.F., Zhou, M.F., Li, J.W., Wu, F.Y., 2008. Association of Neoproterozoic A- and I-type granites in South China: Implications for generation of A-type granites in a subduction-related environment. Chemical Geology 257, 1–15.
Zhao, J.L., Qiu, J.S., Li, Z., Li, Y.L., 2012. Petrogenesis of the Taiwushan granite pluton in Fujian Province: constraints from zircon U-Pb ages and Hf isotopes. Acta Petrologica Sinica 28 (12), 3938–3950 (in Chinese with English abstract).
Zhao, J.L., Qiu, J.S., Liu, L., Wang, R.Q., 2015a. Geochronological, geochemical and Nd–Hf isotopic constraints on the petrogenesis of Late Cretaceous A-type granites from the southeastern coast of Fujian Province, South China. Journal of Asian Earth Sciences 105, 338–359.
Zhao, Z.F., Gao, P., Zheng, Y.F., 2015b. The source of Mesozoic granitoids in South China: Integrated geochemical constraints from the Taoshan batholith in the Nanling Range. Chemical Geology 395 (2015), 11–26.

Zhou, Z.X., 1988. Chemical characteristics of mafic mica in intrusive rocks and its geological meaning. Acta Petrologica Sinica 4, 63–73 (in Chinese with English abstract).
Zhou, X.M., Li, W.X., 2000. Origin of late Mesozoic igneous rocks in southeastern China: implications for lithosphere subduction and umderplating of mafic magmas. Tectonophysics 326, 269–287.
Zhou, X.M., Sun, T., Shen, W.Z., Shu, L.S., Niu, Y.L., 2006. Petrogenesis of Mesozoic granitoids and volcanic rocks in South China: a response to tectonic evolution. Episodes 29, 26–33.
Zhu, D.C., Mo, X.X., Niu, Y.L., Zhao, Z.D., Wang, L.Q., Liu, Y.S., Wu, F.Y., 2009. Geochemical investigation of Early Cretaceous igneous rocks along an east–west traverse throughout the central Lhasa Terrane, Tibet. Chemical Geology 268, 298–312.
Zhu, W.G., Zhong, H., Li, X.H., He, D.F., Song, X.Y., Ren, T., Chen, Z.Q., Sun, H.S., Liao, J.Q., 2010. The early Jurassic mafic–ultramafic intrusion and A-type granite from northeastern Guangdong, SE China: Age, origin, and tectonic significance. Lithos 119, 313–329.